Alma Mater Studiorum - Università degli Studi di Bologna

DOTTORATO DI RICERCA IN
MECCANICA E SCIENZE AVANZATE DELL'INGEGNERIA

Ciclo **XXVI**

Settore Concorsuale di afferenza:
09/C1 INGEGNERIA DELLE MACCHINE E DEI SISTEMI ENERGETICI

Settore Scientifico disciplinare:
ING-IND/08 MACCHINE A FLUIDO

Towards Centrifugal Compressor Stages Virtual Testing

Presentata da:
Dott. Ing. Emanuele Guidotti

Relatore
Chiar.mo Prof. Ing. Giovanni Naldi

Coordinatore Dottorato
Chiar.mo Prof. Ing. Vincenzo Parenti Castelli

Esame finale anno 2014

A thesis submitted to the
Graduate School
of the University of Bologna
in partial fulfillment of the
requirements for the degree of

Ph.D.

in the Department of Industrial Engineering
of the College of Engineering

By

Emanuele Guidotti
B.S., Mechanical Engineering
University of Bologna, Italy, July 2006
M.Sc., Aerospace Engineering
University of Cincinnati, U.S.A., July 2008

Committee Chair: **Professor Giovanni Naldi**

'Essentially, all models are wrong, but some are useful.'

George E. P. Box

ABSTRACT

Requirements for centrifugal compressors performance continue to increase. To this intent, prediction tools need to be at the state of the art to assess performance variations between different designs and/or to predict, within tight tolerance, single stage or multi-stage machines for design verification. Furthermore, the complex flow phenomena inside the different components of centrifugal compressor stages need to be fully understood to allow aerodynamicists to design new stages with increasing performance but at the same time to produce reliable and robust machines.

However, flow features inside centrifugal compressor stages are very complicated to simulate with numerical tools due to the highly complex geometry and varying gas conditions all across the machine. For this reason, a big effort is currently being made to increase the fidelity of the numerical models during the design and validation phases. Computational Fluid Dynamics (CFD) plays an increasing role in the assessment of the performance prediction of centrifugal compressor stages. Historically, CFD was considered reliable for performance prediction on a qualitatively level, whereas tests were necessary to predict compressors performance on a quantitatively basis. In fact "standard" CFD with only the flow-path and blades included into the computational domain is known to be weak in capturing efficiency level and operating range accurately due to the under-estimation of losses and the lack of secondary flows modeling. This research project aims to fill the gap in accuracy between "standard" CFD and tests data by including a high fidelity reproduction of the gas domain and the use of advanced numerical models and tools introduced in the author's OEM in-house CFD code. In other words, this thesis describes a methodology by which virtual tests can be conducted on single stages and multistage centrifugal compressors in a similar fashion to a typical rig test that guarantee end users to operate machines with a confidence level not achievable before. Furthermore, the new "high fidelity" approach allowed understanding flow phenomena not fully captured before, increasing aerodynamicists capability and confidence in designing high efficiency and high reliable centrifugal compressor stages.

ACKNOWLEDGMENTS

When a journey is completed, one of the pleasure is to look over the past and remember all the people who have been present and supported me along this long but exciting road.

It is very difficult to overstate my gratitude to my Ph.D. advisor Prof. Giovanni Naldi who helped to make turbomachinery and CFD fun for me. He always enabled me to face the hard work with a smile on the lips. He has been an exceptionally good leader and motivator. He has provided me encouragement, good teaching and lots of good ideas. I am really glad that I have come to get know you in my life.

I love all the professors I have deal with at both University of Bologna and University of Cincinnati but a special mention goes to Prof. Orkwis and Prof. Turner. I owe a debt of gratitude to both of you.

I'll always be grateful to GE Oil&Gas Nuovo Pignone for letting me publish all the material presented in this thesis and for the financial support. I'll be forever in debt to my former and current managers at GE OIL&GAS Nuovo Pignone Libero Tapinassi and Tommaso Dante Rubino for their sound advices and their constructive and critical spirit.

Thanks to my friends, which are too many to mention (a thesis has a page size maximum, guys). So because the list might be too long and by fear of leaving someone out, I will simply say thank you very much to you all. Some of you, anyway, are quite lucky: thank you Pietro, Sandro and Andrea.

My deepest gratitude goes to my parents Rolando and Aurora and to my brother Christian and to Zietta and all my relatives. They bore me, raised me and loved me. They have provided everything that one could hope for in a family. And in the end my parents has taught me everything that I truly need to know in life.

I dedicate this thesis to Paola and Martina. This thesis is yours too, and so the spirit behind it, which in the end is everything. Whenever I try to describe my feelings for you...no matter what I come up with, it only seems to capture half of the story.

———

Contents

List of Figures

List of Tables

Nomenclature

Symbol	Units	Description
Cp	$-$	Static pressure recovery coefficient
D	m	Diameter
$\dot{m}$	kg/s	Mass flow rate
Mu	$-$	Peripheral Mach number
P	Pa	Pressure
Q	m^3/s	Volumetric flow rate
R	$J/(kg*K)$	Gas constant
T	K	Temperature
U	m/s	Peripheral speed
V	m/s	Absolute velocity
YAW	$degree$	Absolute flow angle
$y+$	$-$	Dimensionless wall distance
Z	$-$	Compressibility factor

Greek Symbols

Symbol	Units	Description
ϵ	m^2/s^3	Turbulent dissipation
Φ	$-$	Flow coefficient
γ	$-$	Ratio of specific heats
η	$-$	Efficiency
κ	m^2/s^2	Turbulent kinetic energy
μ	$Pa*s$	Viscosity

θ	$-$	Circumferential direction
ρ	kg/m^3	Density
τ	$-$	Work coefficient
ω	$1/s$	Specific dissipation rate
ξ	$-$	Total pressure loss coefficient
ψ	$-$	Head coefficient

Subscripts and superscripts

in	Inlet component
M	Meridional component
out	Outlet component
p	Polytropic
r	Radial component
s	Static quantities
t	Total quantities
1	Impeller inlet
2	Impeller exit

Acronyms

BPF	Blade Passing Frequencies
CAD	Computer Aided Design
CAES	Compressed Air Energy Storage
CCS	Carbon Capture and Sequestrations
CFD	Computationa Fluid Dynamics
CTL	Coal To Liquids
DNS	Direct Numerical Simulation
EGR	Entropy Generation Rate
EOR	Enhanced Oil Recovery
FCC	Fluid Catalytic Cracking
FFT	Fast Fourier Transform
FRAPP	Fast Responce Aerodynamics Pressure Probe

GGI	General Grid Interface
GMBS	Global Multi-Block Surfaces
GTL	Gas To Liquids
IGCC	Integrated Gasification Combined Cycle
IGV	Inlet Guide Vanes
JST	Jameson-Schmidt-Turkel
KL	Kato-Launder
LES	Large Eddy Simulation
OEM	Original Equipment Manufacturer
RANS	Reynolds Averaged Navier Stokes
URANS	Unsteady Reynolds Averaged Navier Stokes
SST	Shear Stress Transport

Chapter 1

Introduction

In the recent years, Computational Fluid Dynamics (CFD), has evolved enormously and it is now used extensively by turbomachinery OEMs in designing the varoius components.

Flow phenomena inside centrifugal compressor stages are very complicated to simulate with numerical tools due to the highly complex geometry and varying gas conditions all across the machine. For this reason, the accuracy of CFD, for designing and predicting centrifugal compressors performance is currently under a controversial and stimulating debate.

1.1 Motivation

The idea of this work was born with the intent to push CFD capabilities towards virtual testing of centrifugal compressor single and multistage machines.

Market trend requires centrifugal compressors OEMs to produce machines with continuously increasing performance and end users to safely operate the compressors. In particular, this translates in a constant effort for aerodynamicists to design new stages with increasing flow capacity and higher peripheral Mach number but at the same time to produce reliable and robust machines. The accuracy of prediction and design tools is critical for the purpose.

On one hand, thermodynamic tests on single and multistage centrifugal compressors are commonly conducted in centrifugal compressor OEMs as per API-617 to assess machines performance. On the other hand, prediction tools need to be at the state of the

art to predict, within extremely tight tolerances, compressor performance and avoid expensive reworking during testing phase.

Historically, CFD was considered reliable for performance prediction on a qualitatively level, whereas tests were necessary to predict compressors performance on a quantitatively basis. In fact, "standard" CFD with only the flow-path and blades included into the computational domain is known to be weak in capturing efficiency level and operating range accurately due to the under-estimation of losses and the lack of secondary flows modeling.

In the vision of the author, CFD is nowadays mature enough to represent a reliable tool for accurate centrifugal compressor performance prediction when an high fidelity reproduction of the geometry and advanced numerical models are used into the simulations.

This research project aims to fill the gap in accuracy between "standard" CFD and tests data by including a high fidelity reproduction of the gas domain and the use of advanced numerical models introduced in the author's OEM in-house CFD code. In other words, this thesis describes a methodology by which virtual tests can be conducted on single stages and multistage centrifugal compressors in a similar fashion to a typical test rig that guarantee aerodynamicists to design machines and end users to operate machines, with a confidence level not achievable before.

1.2 Overview

In the past few decades, significant developments have been achieved in the numerical models and the associated CFD algorithms. Furthermore, in the author's OEM, a big effort has been done in the recent years, to develop automatic and robust meshing tools that allow the aero designers to model additional features not included before into the computational domain. Combined with the rapid developments in computer hardware in both speed and memory which are becoming increasingly available at affordable prices, the simulation of complete test rigs or even full compressors are increasingly becoming a reality.

Several centrifugal compressor single stages, ranging across different inlet flow coefficients and peripheral Mach numbers, applied to disparate processes (e.g. LNG, pipeliners, barrel compressors, etc), as well as applications of multistage compressors, were selected as test cases for this study. Both steady and unsteady simulations were conducted in order to fully capture the time averaged and time accurate operating conditions. Moreover, detailed geometrical features like fillets and leading edge shape as well as the entire secondary

cavity flows system were faithfully reproduced in the computational domain and advanced numerical models were used in the setup with accuracy not possible before.

CFD predictions were compared with test results regarding both overall performance and detailed flow features showing a very good agreement, not found in open literature for closed impeller stages. Furthermore, the new "high fidelity" approach allowed understanding flow phenomena not fully captured before, increasing aerodynamicists capability and confidence in designing high efficiency and high reliable centrifugal compressor stages. The increment in performance prediction accuracy with respect to "standard" CFD is noticeable. Advantages of this approach is the reduced cost with respect to tests and the possibility to virtually instrument the machine all along the computational domain where it is not possible in the real compressor.

This thesis delves into the details of the CFD accuracy by introducing innovative methodologies and capabilities for tri-dimensional numerical simulations. Several test cases have been simulated and results will be presented throughtout this work to assess computational capabilities comparing predictions with test data. Finally a clearer understanding of flow features inside the centrifugal compessors is claimed.

- Chapter 2 presents the details about the selected test cases and the strategy for numerical validation.
- In chapter 3 the experimental setup and test data are provided as well as a description of the GE OIL&GAS testing capabilities
- In chapter 4 is presented the calculations setup as well as a detailed explanation of the theory behind the numerical models and tools used.
- In chapter 5 the results of the present work and the comparison between the experimental data and the numerical simulations are shown. Furthermore, a review of the implications of geometrical and numerical models with computational accuracy is presented.
- Chapter 6 shows the details and the explanation of flow phenomena and secondary flows inside centrifugal compressors stages.
- Finally chapter 7 surveys the results from all the chapters and summarizes them. Future directions for research and improvements to the current work are also suggested.

All throughout the thesis, a complete literature review of the current state of the art in CFD simulations for centrifugal compressor stages is presented for each specific argument.

Chapter 2

Test Cases Description

In the OIL&GAS market, centrifugal compressors are used extensively for very different applications and in the most variable operating conditions. Centrifugal compressors can be classified based on applications, casing types, number of stages, etc. Furthermore, each single stage is classified based on some adimensional parameters.

Validation of the numerical models in this reasearch work has been conducted on several different geometries, single and multistage compressors, different applications, different working gas, different operating conditions like inlet pressure and so on.

2.1 Centrifugal Compressors Classification

Currently a separation in upstream, midstream and downstream sectors is often used to categorize the different applications. A rough classification of the different sectors is given here:

- Upstream: oil & gas i.e. gas lift, gas export, gas injection, gas gathering, gas treatment, gas processing, CO2 injection, LNG, boil off, gas transport, liquefied petroleum gas.
- Midstream: gas transport, gas storage, fuel gas, CAES.
- Downstream: refineries, fertilizers, chemical & petrochemical, i.e. hydrogen production, hydrogen recovery, hydro cracking. Desulfurization, FCC, propane dehydration, methanol, olefins, IGCC, Coal-to-Liquids, GTL-Syngas, ammonia, urea, nitric acid. Industrial gases: air separation, nitrogen, oxygen, paper, coke oven, GTL, CTL.

- Power generation: fuel gas, CCS.

A classification of centrifugal compressors based on the casings is:

- Vertically split casings
- Horizontally split casing
- Barrel compressors
- Overhung/integrally geared compressors

Moreover, the different compressors can be single stage, multistage with single or multiple sections, back to back and so on.

As already highlighted before, gas and operating conditions can vary greatly: inlet pressure can be from atmosferic to several hundred bar, gas can range from single component, light gases like hydrogen to mixtures of heavy hydrocarbons.

A common classification for single stage description is given by defining the adimensional parameters Φ (inlet flow coefficient) and Mu (peripheral Mach number).

The flow coefficient and peripheral Mach number are defined as equations (2.1) and (2.2) respectively.

$$\Phi = \frac{4 \times Q_{t,1}}{\pi \times D_2^2 \times U_2} \tag{2.1}$$

$$Mu = \frac{U_2}{\sqrt{\gamma \times R \times T_{t,1}}} \tag{2.2}$$

Where $Q_{t,1}$ is Volumetric flow rate (calculated using total density) at impeller inlet.

2.2 Test Cases Selection

As described in the previous paragraph, the applications, working gases, inlet conditions and geometries can vary greatly in centrifugal compressors. For this reason to validate the accuracy of current CFD it was necessary to select different cases. Furthermore, different flow phenomena are predominant depending on the stage type; e.g. bi-dimensional impellers are dominated by leakage and friction losses, instead tri-dimensional high flow coefficient stages by curvature and secondary flows losses. To this intent, several single stage

and multistage centrifugal compressors were selected for numerical models validation and comparison with test data, ranging across a full spectrum of different flow coefficients and peripheral Mach numbers. In particular below a summary of the different cases is provided:

- Working gas: air, CO2, propane, methane, hydrogen, nitrogen, ammonia, refrigerant gases, hydrocarbon mixtures.
- Inlet pressure: from atmosheric up to several tens of bar.
- Inlet temperature: from several degrees below zero up to several tens of degrees Centrigade.
- Mach number: from highly subsonic flows up to transonic ones.
- Inlet flow coefficient: from very small bi-dimensional impellers up to mixed flow tridimensional ones.

Furthermore, both single stage and multistage machines have been studied, both over-hung, vaned diffusers impellers with inlet guide vanes and vaneless intermediate stages have been simulated.

Figures 2.1 and 2.2 show the different cases used to validate the CFD methodology presented here divided respectively on the plane peripheral Mach number-inlet flow coefficient (Mu-Φ) and compressor inlet temperature-inlet pressure ($T_{in} - P_{in}$) respectively. It can be seen that the full range of peripheral Mach numbers and inlet flow coefficients of most common industrial applications of centrifugal compressors has been covered. Moreover, if on one hand inlet atmospheric conditions of pressure and temperature are the ones used the most in single stage validations, Reynolds effect has been also studied with several validation cases, both on pressurized test rigs and full scale type 2 and string tests.

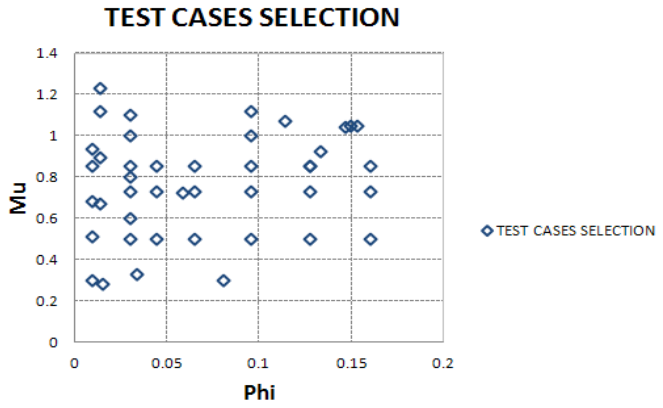

Figure 2.1: Test cases on plane Mu-Φ.

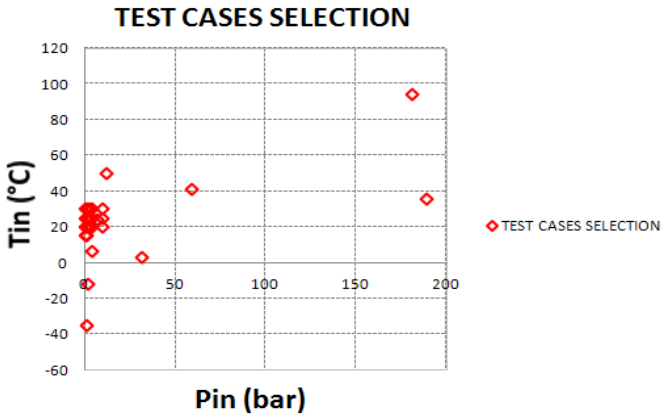

Figure 2.2: Test cases on plane $T_{in} - P_{in}$.

Chapter 3

Experimental Setup and Data

Depending on the test case, the experimental verification of compressor performance was done at the GE Oil&Gas testing facilities either in Florence or Massa. In particular, in Florence at the Oil&Gas Technology Laboratory (OGTL) all the single stage tests were performed whereas the type 2 tests were done in full scale test rigs in the same plant. At Massa testing facilities the string tests were operated.

3.1 Test Rigs Description

All the tests have been performed by following API-617 regulations. In the following paragraphs the description of the different test rigs will be shown with the overlapping areas between the different test benches setup clearly highlighted.

3.1.1 Single Stage Test Rig Description

A typical single stage test bench, whose test cell is depicted in Fig. 3.1, consists of a closed loop rotating rig, which is employed for performance measurements of many centrifugal compressor designs; further details can be found in [1]. The test rig can be used for both intermediate stage configuration or axial inlet configuration. For the intermediate stage configuration, a multistage compressor is simulated through a "pseudo-stage" in the flow-path upstream of the impeller. This is included in order to provide flow profiles at the impeller inlet typical of that expected in a multistage environment. The pseudo-stage consists of a set of pre-swirl vanes followed by a return channel. Instead for the axial inlet configuration, the test cell is modified according to Fig. 3.2 where inlet guide vanes

and an outlet scroll replace the upstream pseudo-stage and the downstream return bend respectively. The test rigs are instrumented so as to allow flange-to-flange measurements, single component performance evaluation (e.g., impeller efficiency and head, diffuser recovery and losses, etc.), as well as the detection of the occurrence of stall and surge (through dynamic probes installed for this purpose). Measurements are taken at various locations throughout the test rig. The instrumentation used is well established and can be tailored to suit the needs of a specific study. For the purpose of this discussion, only the measurement apparatus of direct relevance to performance evaluation is discussed. Pressure, temperature, flow angle and velocity measurements were performed at each of the measurement locations throughout the compressor. According to Fig. 3.1 and Fig. 3.2, the main measurements sections are indicated as:

- Section 00: Stage inlet/IGV inlet
- Section 10: Impeller inlet
- Section 20: Impeller outlet/diffuser inlet
- Section 40: Diffuser outlet/return channel or scroll inlet
- Section 60: Stage outlet/return channel or scroll outlet

Single stage test rigs are usually operated in similitude conditions with real machines due to the impossibility to opearte at the same inlet pressure and with the same working gas of on site machine.

3.1.2 Type 2 and String Test Rigs Description

Type 2 performance tests is conducted on real machine geometry. It can be considered as a laboratory-type fluid test on real machine to confirm fluid dynamic characteristics of the compressor. It permits the use of a substitute test gas and accepts extensive deviations between test and specified operating conditions. There are only a few limits on some essential gas dynamic parameters of test conditions (compare to specified operating conditions). Specific volume ratio and flow coefficient should be within around 5% deviations. There are some limits on machine Mach number and machine Reynolds number. The test speed, capacity, mass flow, pressures, temperatures, power, etc are often totally different

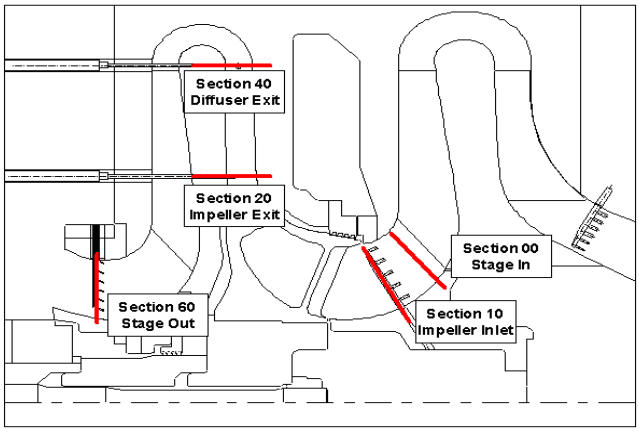

Figure 3.1: Test Rig setup in intermediate stage configuration.

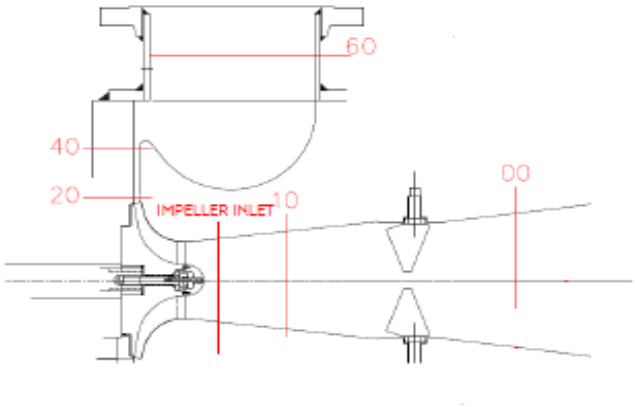

Figure 3.2: Test Rig setup in axial inlet configuration.

from the specified operating condition speed. In Type 2 test, a suitable gas is identified which does not lead to excessive power or discharge temperature and is readily and cheaply available. Substitute gas such as air, nitrogen, CO2, CO2/He mixes, fuel gas, etc are used. Safe operating speed, critical speeds, maximum allowable pressures, allowable temperatures and other machine limits are considered in test condition selection. In type 2 test, test Reynolds number is different compared to specified operating condition but it is still within certain limits to keep governing friction formulations the same (same model and flow regime). Based on theory, a correction to the test results is applied based on available gas dynamic knowledge to estimate the friction effects of compressor performance in specified operating

condition. All correction formulations are available in API-617 for estimation.

Instead a string test type 1 performance test is actually a shop performance test in anticipated site condition. It is conducted with same gas as site (same gas with molecular weight deviation below 2%). Generally pressure, temperature, compressor speed and capacity permissible deviations are below around 4-8%.

Type 2 and string tests are, as expected, less instrumented than single stage model tests. Usually, inlet and outlet sections are fully instrumented and vibration detection is performed all throughout the test duration. On some special cases, like prototype cases, compressor is heavily instrumented to have also inter-stage or inter-component measurements whenever possible.

Figures 3.3 and 3.4 show the GE OIL&GAS testing facilities for both type 2 and string tests on centrifugal compressors, respectively in Florence and Massa.

Figure 3.3: Type 2 centrifugal compressors test facilities at GE OIL&GAS in Florence.

3.2 Measurement Techniques

Measurement techniques and instrumentations are common to all the different test rigs with particular indications for each setup given in the previous sections.

Total pressure measurements are made with Kiel probes, static pressure measurements are made using wall taps (both at the hub and at the shroud) and shielded J-type thermocouples are used for total temperature measurements. Flow angles are measured either with three-hole or five-hole probes, depending on the expected three-dimensionality of

Figure 3.4: String test centrifugal compressors test facilities at GE OIL&GAS in Massa.

the flow. To minimize the intrusiveness and increase the resolution, axial-radial actuators and a rotating conveyor (where instrumentation is installed) can be employed. The use of multiple probes rake or single probe with traversing system depends on the fow channel size; in fact for narrow channel is preferred to employ one single probe to minimize the aerodynamics blockage given by the probe itself. Moreover, probe actuators allow both maximum recovery of Kiel probes and "nulling mode" operation for multi-hole probes. The flow rate is measured with an orifice following the EN ISO 5167-1 standard, while the rig rotating speed is measured using a magnetic pick-up based key-phasor. The uncertainties at the 95% confidence level associated with the steady measurements of each section are collected in Table 3.1. The measurements accuracy, evaluated usign a calibrated nozzle, is $\pm 0.5\%$ of the kinetic head for both the total and static pressure and $\pm 0.2°$ for the yaw angle.

3.3 FRAPP Probe

The FRAPP (Fast Responce Aerodynamics Pressure Probe) has been recently introduced in the Oil&Gas Technology Laboratory (OGTL) and is employed in single stage measurements at the exit of impeller, i.e. section 20, in order to obtain a highly detailed reconstruction of flow field. The FRAPP measurement concept arises from the matching of classical pneumatic directional probes and piezoresistive fast-response pressure transducers. While the former, like a cobra probe and 5 hole probe, can provide information about an unknown steady flow field, the latter offers fast-response, miniaturization, reliability and

Measurement	Section	Absolute Uncertainty
Temperature	10	± 0.2
Pressure	10	± 35 Pa
Yaw Angle	10	± 0.5 deg
Temperature	20	± 0.2
Pressure	20	± 155 Pa
Yaw Angle	20	± 0.5 deg
Pitch Angle	20	± 0.5 deg
Temperature	40	± 0.2
Pressure	40	± 155 Pa
Yaw Angle	40	± 0.5 deg
Temperature	60	± 0.2
Pressure	60	± 155 Pa
Yaw Angle	60	± 0.5 deg

Table 3.1: Measurement uncertainties.

low cost. This combination of features allows the unsteady evolution of the flow field to be measured. Despite the number of different configurations available, the highest degree of miniaturization is achieved with single-sensor probes, which allow the measurement of the 2D flow field in a plane normal to the probe stem. Since the probe has a single hole, only one measurement at a time can be performed. The flow field is then reconstructed by re-arranging three pressure measurements at different angles of rotation around the probe axis, thus virtually reproducing the three-hole probe technique.

The probe considered here was developed around a commercial miniaturized pressure sensor (Kulite XCQ-062, full scale 25 psi) to ensure high reliability, low cost and simplified manufacturing of the probe heads. The probe concept was developed at the Politecnico di Milano over the last decade. The transducer is installed co-axially with the probe head to obtain a minimum probe head diameter of 2.0 mm. The final probe spatial resolution, defined as the physical distance between the extreme positions of the tap, is 1.5 mm. The single pressure tap on the probe head has a diameter of 0.3 mm. Detailed information regarding FRAPP technology can be found in [2] and [3].

The instantaneous pressure signals is acquired at 1 MHz for a period of 1 second. Raw pressure data are phase-locked to the rotor wheel and then phase-averaged to obtain 40 intervals on a single rotor-blade passing period (BPP). As a final step, the flow properties are derived by combining the different phase-averaged pressures.

The unsteady flow quantities, originally measured in the absolute frame, are further converted into relative quantities making use of the time-averaged total temperature measured at station 20. Furthermore, other quantities can be derived, even if under some assumptions, like the turbulent kinetic energy.

A validation of the FRAPP based technique was successfully carried out in a previous activity where a comparison between a FRAPP and a pneumatic 5-hole probe was made [4]. Good agreement was observed in terms of both average values over the entire flow field and hub-to-shroud profiles as also shown in Table 3.2 where the percentage errors for the average results are listed. However, no detailed information or detailed flow-field reconstruction can be obtained with a 5-hole probe, whereas FRAPP can actually provide information about the two-dimensional flow field in terms of total pressure, static pressure and yaw angle. Thanks to the unsteady character of this techniques, FRAPP data can be used to derive the "steady" flow field in the relative frame at the rotor exit.

Measurement	Percentage error (FRAPP-5H)/5H
Total Pressure	0.10%
Static Pressure	1.80%
Yaw Angle	0.70%

Table 3.2: Percentage differences between FRAPP and 5-Hole Probe .

Figure 3.5 shows the dynamic pressure probe, while Fig. 3.6 depicts the FRAPP installed at the impeller exit in a typical test rig configuration; the red circle shows the FRAPP location.

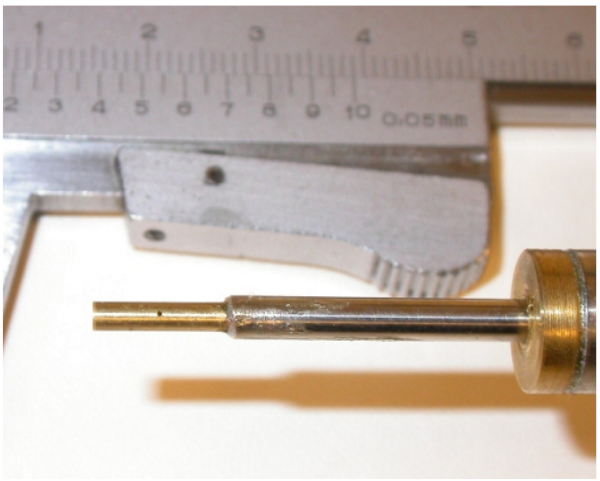

Figure 3.5: FRAPP probe.

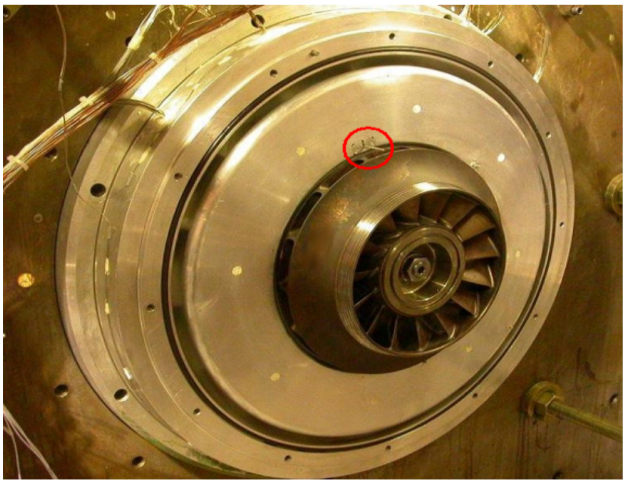

Figure 3.6: FRAPP installed at the exit of a centrifugal impeller.

Chapter 4

Numerical Models

The three-dimensional and viscous nature of the flow field inside a modern high speed centrifugal compressor stage is difficult to simulate with numerical models. Nevertheless, during design phase, is fundamental to correctly predict the flow behavior and the corresponding performance of the stage to validate the design accurately. Software tools, ranging from simple one-dimensional to highly complex fully three-dimensional are used to assess this issue. The advantage of one-dimensional tools is that they are fast and reliable for an overall screening of the design space and overall performance prediction. However, accurate three-dimensional computational models are necessary to simulate the flow structures that are not captured by simpler models. The drawback of such complex tools is the execution time, that especially with the increasing complexity in modeled features, sometimes can be not affordable during design space exploration. In addition, for radial machines, the high curvature of streamlines makes the CFD computations even more difficult to simulate with a good accuracy with respect to axial machines. Many validation cases are available in open literature on centrifugal compressor stages like [5], [6], [7], [8], [9] to name a few. However they are mainly related to open impellers or, for closed ones, they lack in capturing losses generation correctly and so the overall performance of the stages due to a not fidelity representation of the real machine and environment.

4.1 Cavity Modeling in Centrifugal Compressors

In closed centrifugal compressor impellers like the ones used as test cases in this study, a gap remains between diaphragms and impeller trailing edge on both hub and shroud

sides. Due to the high pressure at the trailing edge location those cavities need to be sealed in order to avoid the flow passing through. The cavity at shroud side is usually connected to the impeller leading edge and labyrinths are used to reduce as much as possible the leakage. On the hub side the trailing edge gap is connected via a cavity up to the return channel trailing edge. Labyrinths are used there as well. In over-hung impellers, the rear cavity can be sealed or in a back-to-back configuration, is connected with the opposite impeller to balance the axial thrust. In single stages, the back cavity can also used to balance inlet and outlet pressure connecting the two parts. In mutistage machine the last impeller is often connected to the inlet through a balancing line.

Leakage flows play a big role in the correct prediction of flow behavior in centrifugal compressors. Up to few years ago, the modeling of cavities in centrifugal compressor stages was not adopted and only the main flow-path was simulated. A new approach using appendages and source terms has been proposed by this author in [10]: this enhanced model allows to correctly capture overall performance and flow features with an almost negligible increase in computational and user time with respect to the model without any cavity included. However, an additional source model needs to be added and a flow network resolved by external dedicated tools for each operating point. Furthermore, correlations used in the tools need to be tuned for dedicated cases; 1D models are know to be weak in correct windage losses prediction. Moreover the flow features inside the cavities are not simulated and reproduced. In fact the knowledge of the flow inside the impeller cavities is fundamental, not only for the aerodynamic designers but also for the mechanical and rotordynamic assessments of the stage. Axial thrust, aeromechanical behavior, swirl brakes design, seals design and geometry optimization can be evaluated and predicted by the numerical tools if the entire cavities are included in the model.

Few studies are available on centrifugal compressors with full cavities modeled in open literature. Validation studies are mainly related to open impellers. For open impellers, some attempts are reported with the aim to simulate the effects of flow control devices on stage operating range. In the studies from Hunziker [11] and Tamaki [12], the flow analysis inside such bleed slots for internal recirculation are shown and the numerical results with respect to baseline configuration without control devices are discussed. Sun et al. [13] simulated a backside cavity of an open centrifugal compressor impeller using a source terms approach. The effects of the hub cavity on the impeller flow field have been reported. For closed impeller centrifugal compressor stages the study from Mischo et al.

[14] shows a comparison of different shroud cavities geometry and the influence on impeller performance as well as comparison of overall performance of the stage with test data. Wang et al. [15] studied the effects of different cavities geometries on overall performance in a low flow coefficient centrifugal compressor stage. In the recent past, the modeling of cavities in centrifugal compressor stages using appendages and source terms was presented by Guidotti et al. [10]. The main limitations in this approach is the reliability of tuned 1D tools for correct prediction of the source terms at each operating point of the stage. The influence of with and without full cavity modeling at design point for one flow coefficient stage on overall performance and flow field was shown in an earlier activity by Guidotti et al. [16] and [17] and reported a substantial improvement in the accuracy of the prediction with full cavity numerical model on a centrifugal compressor stage. Satish K. et al. [18], following the same approach, showed an accurate agreement between advanced test data and numerical prediction on different flow coefficient centrifugal compressor stages using steady computations. Lettieri et al [19] also showed a good agreement between test data and CFD with cavity modeling.

4.2 Computational Setup

Results presented in this thesis were obtained by using the GE in-house CFD code TACOMA. TACOMA (Turbine And COMpressor Analysis) is a GE proprietary code used for computational fluid dynamics simulations on axial and radial turbomachinery. TACOMA is a 3D multi-block, multi-grid, structured, non-linear and linear Euler/Navier-Stokes solver for turbomachinery blade rows. TACOMA is a cell-centered explicit flow solver based on the so-called JST scheme [20]. Details of the scheme as well as validation cases can be found in [21] and [22]. The solution is obtained via a multi-step Runge-Kutta explicit time marching scheme with convergence acceleration via local time steps, residual averaging, and V-cycle or W-cycle multigrid. In the present analysis, steady and unsteady 3D Reynolds-Averaged Navier-Stokes (RANS and URANS) equations are solved. Both the two equations $\kappa - \omega$ turbulence model developed by Wilcox [23] and the variation SST were used in the computations. TACOMA uses by default the production modification of Kato and Launder instead of the original one [24]. Also the curvature correction model that was found to be useful on centrifugal compressor stage analysis as shown by Smirnov et al [7] has been implemented into the code. Previous validations and modeling experiences with TACOMA

on centrifugal compressor stages can be found in [25], [26], [27], [10], [28], [16], [17] and [29] .

4.3 Computational Grid

Two different grid domains were meshed for each airfoil. In particular, the geometry of the compressor main flow-path was modeled with the Numeca grid generator Autogrid by importing the flow-path and sections at different spanwise locations for all the airfoils. The geometry of the stage was exactly replicated from the test rig including fillets. Structured grids for impeller, diffusers and/or return channel were generated. Instead the cavities domains were meshed by a recently developed in-house GE tools. Finally all the blocks were merged. The new automated in-house tools for cavity meshing requires a very short amount of additional user time. The base airfoil grid is linked to a CAD software where the axis-symmetric shape of the cavity is reproduced; the meshing tools uses the two domains to mesh the cavity once some topology parameters are provided in a text file. The possibility inside the new tools to split and merge the different blocks allows the user to create very accurate grids in different domains and then manipulate them. Also the possibility to create templates for different centrifugal stages is beneficial for repeating designs. The computational domain includes, depending on the test case, impeller, vaneless or vaned diffuser, return channel, hub cavity and shroud cavity, double inlet, balancing line, etc.

The entire CFD domain including cavities for a typical one stage simulation is shown in Fig. 4.1. From right to left, it can be seen in sequence the preswirl, deswirl, impeller and return channel vanes as well as the two cavities connecting impeller trailing edge to impeller leading edge shroud side and return channel to impeller hub side.

The meshed forward and back sides cavities before merging are shown in Fig. 4.2.

Details of the grid inside the cavities including labyrinth seals at both shroud and hub sides are shown in Fig. 4.3 and Fig. 4.4 showing the very good grid details including a correct boundary layer grid clustering.

For multistage applications, the different computational stage domains are stacked in sequence. Profiles are exchanged through the different rotating/not rotating domains with tangential averaging of main quantities at interfaces. To have a fairly similar numerical resolution along the span direction and avoid numerical inaccuracies, a similar grid is targeted on both sides of the interface. An example of a multistage application is showed in

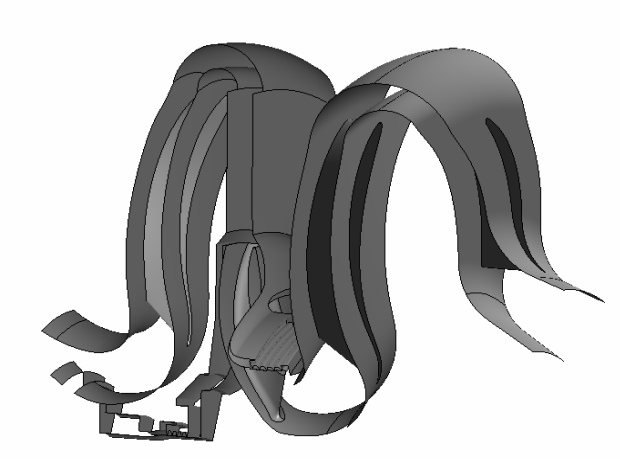

Figure 4.1: CFD domain including cavities for single stage test rig.

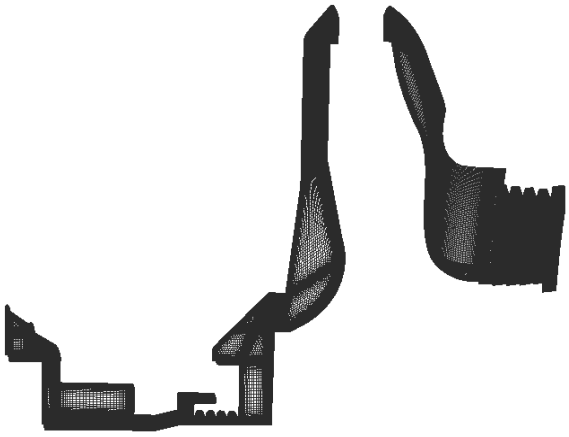

Figure 4.2: CFD Forward and back sides cavities grids before merging.

figure 4.5.

The grid size for each airfoil domain is the result of many grid sensitivity studies and cases validation performed during past years in the author's OEM like the ones in [10], [16], [17], [18] [25], [26] and [27]. To give a rough estimation of the sensitivity study resuts, it has been found that below about 200k cells for each airfoil domain the main flow features are not captured at all. Between 200k and 500k cells only blade loading distribution is well reproduced. Up to 1000k cells are necessary for a good matching between numerical results

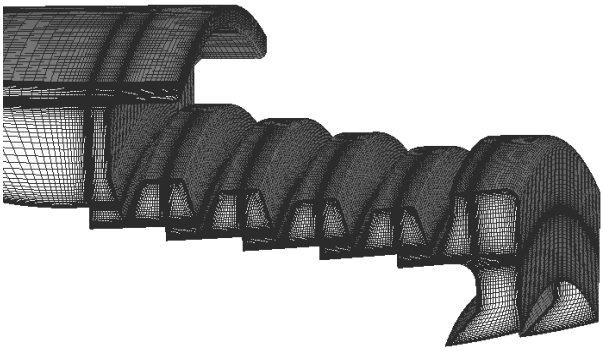

Figure 4.3: Cavity domain details shroud side.

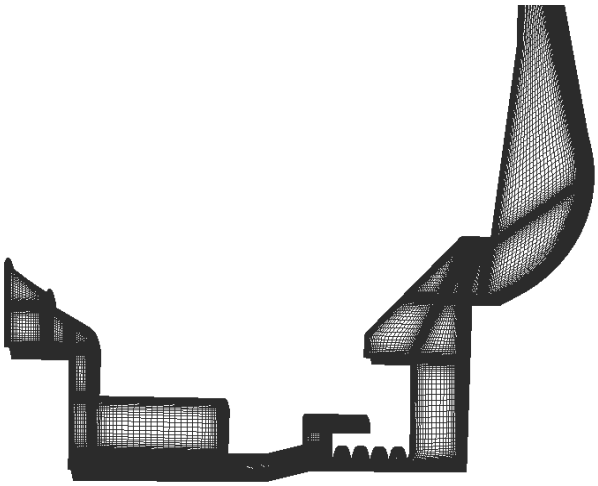

Figure 4.4: Cavity domain details hub side.

and test measurements on exit angles profiles. More than 1000k cells are mandatory for loss generation and mechanisms assessment. A flat response of results was found at about 2.5 million of computational cells for each airfoil main flow-path domain. Furthermore the increment in computational time and memory requirements with included meshed cavities with respect to only main flow-path computations is about 30%. As already stated, negligible addition in user time is required thanks to the new in-house automated tools.

Wall integration is used to capture the boundary layer and computational grids

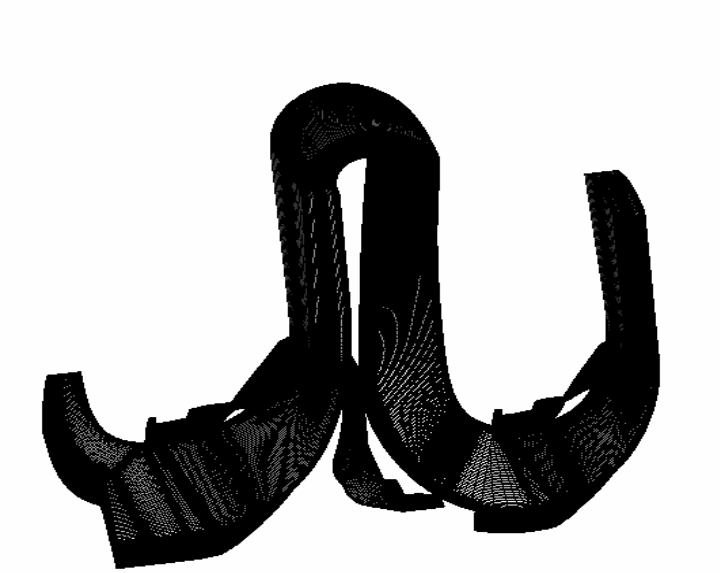

Figure 4.5: Two stages computational domain.

modeled with an average y+ less than 1 on all the wall surfaces to ensure good resolution of viscous sub layer. In particular, to accurately model boundary layer development inside the cavities, the in-house GE meshing tool allows inserting an O type grid block at each wall inside the cavities. TACOMA Global Multi-Block Surfaces (GMBS) interfaces were imposed at few domain interfaces, where one-to-one interface connections are not modeled. At GMBS interface locations, the mesh on both sides was created in order to have fairly similar grid clustering. GMBS (non conformal interfaces) allow not to have a one-to-one connection at interface and also to realize the grid in the airfoil domain without any distortion especially in the area close to the impeller trailing edge where the correct resolution of flow features is mandatory for the correct loss modeling assessment. Airfoil/cavity interface can have blocks extents and grid counts different on the two sides. Different patch count, size and shape can be realized and a user friendly surfaces tagging system has been included. A modification of the CFD code has been necessary to cope with non matching block interface. A new advanced system of donor/acceptor cells across the interface with a cell area weighting flux system has been included. The new feature has been tested inserting non matching blocks in computational domains simulated previously and comparing the results with older block matching computations with no appreciable differences. Then the new system has been extended to cope with cavity domains.

Particular attention was also paid in the main flow domain to correctly defining the mesh close to the leading and trailing edges and to ensuring that enough cells were placed in the passage to capture the main structures of the flow.

4.4 Boundary Conditions

For accurate representation of test setup in CFD computations, the CFD model inlet and outlet locations are maintained same as the experimental setup and the flow profiles at the inlet of the test campaign or previous plenum CFD simulations are applied at the CFD domain inlet and outlet domains. In particular, tangential averaged profiles of total quantities and angles were used at compressor inlet section. Mass flow rate or static pressure conditions were applied at the outlet depending on numerical stability at the different operating conditions. In particular, static pressure at exit can lead to numerical divergence (static instability) close to stall point, so mass flow rate outlet is used close to stall operating condition and static pressure outlet is applied close to choke condition. All the walls are modeled as no-slip and adiabatic. As the heat inside the cavities is dissipated by leakage flows, there is no necessity to use isothermal boundary conditions at cavity walls that is instead necessary when the fluid is stagnant inside the cavities like in the case of a backward cavity in over-hung applications where an o-ring is mounted at the exit.

Numerical computations are performed on single airfoil for the steady computations with periodic boundary conditions. A phase lag boundary condition is used in the tangential direction for the unsteady runs. The algorithm implemented in the GE in-house code TACOMA makes use of the phase-lag boundary conditions introduced by Erdos [30]. The key idea is based on the phase shift methodology, i.e. the assumption that the solution at any particular passage in the blade row can be related to the solution at another passage at an earlier time in the same blade row. This allows modeling of rotor-stator interaction using only a single blade passage in each blade row without the necessity to change blade count between adjacent blade rows and is useful for time-accurate analyses dominated by unsteadiness at the adjacent blade passing frequency. This allows the unsteady simulation to be performed by using only one blade from each of the two rows.

Ideal, linearly variable, or even real gas models have been used in the computations based on the operating pressure and gas type used. Air, carbon dioxide, refrigerant gas, propne, etc. have been setup in the models. For real gas applications, thermodynamics

tables of specific heat, ratio of specific heats and viscosity are linked to the in-house CFD code Tacoma and accessed during the computation. The Benedict-Webb-Rubin equation in the version modified by Starling (BWRS) was used to create the gas table and to calculate the performance.

4.5 Solver Convergence

Complex geometries, multistage coupling, blade-row interactions and many other factors tends to stive CFD convergence capabilities for single and in particular for multistage centrifugal compressor simulations. Furthermore, the introduction of cavity models inside the computational domain represents a challenge for numerical stability due in particular to the very different Mach number between main flow-path and cavities domains that can be even two/three times. GMBS interfaces are used at few domain interfaces, where the nodes on the two sides are not aligned. GMBS interface in TACOMA is modeled to conserve the fluxes across the interfaces. Fluxes on both sides of the interfaces were checked (in the converged solution) and no variations were found up to several decimals. Furthermore for the best results of the interpolation algorithm, the mesh on both sides was made in order to have fairly similar length scales and both sides of the interface fully overlap.

Coupling of main-flow and cavities often produces numerical oscillations that can persist regardless the number of iterations used, expecially at operating conditions where unsteady effects are revelant. In these cases average scalar variables need to be monitored until they reach a stable level. Local adjustments of the grid and/or numerical models and time scale need to be used in order to reach a good convergence and overcome the instabilities due to the different velocities between main-flow path and cavities.

Flow in the cavities travels mostly in the circumferential direction which means that the signal responding to main flow field change takes long time to propagate from one opening of the cavity to the other and as a whole this induces a lower convergence rate with respect to computational model without. Regarding steady computations both mathematical and physical convergence was monitored during the runs and the simulations were stopped when main flow quantities reached a stable pattern. In the unsteady runs Courant number was constantly monitored during the transient computations and time step has been decided to have the average value in an acceptable range, i.e. below 10. However, due to the difference in grid details and velocities inside the different computational domains, a sensible variation

between cavity domains and main flow is expected. In fact the introduction of cavity models inside the computational domain represents a challenge for numerical stability, particularly due to very high difference in Mach number between main flow path and cavities. The average Mach number between main flow path and cavity domains can vary up to 2 to 3 times. Local adjustments of the grid and/or numerical models need to be used in order to reach a good convergence and overcome the instabilities due to the different velocities between main flow-path and cavities. For each time step, convergence has been achieved with main flow quantities residuals down up to 4/5 orders of magnitude. Moreover, the steady converged solution was used to initiate the flow for the transient computations. Suresh et al [31] investigated also the stability of the Phase Lag method on turbomachinery simulations for the TACOMA solver.

Transient methodology is also recommended in cavity flows modeling with high unsteadiness like in the present study to overcome numerical instabilities due to time averaged calculations on inherently unsteady flows. Finally, it is well known that Phase-Lag boundary conditions require approximately an order of magnitude more iterations to converge than full unsteady runs but the possibility to model only one periodic sector for blade row decreases dramatically the time necessary to complete the simulation.

Chapter 5

Numerical Results and Comparison with Test Data

All throughout the following paragraphs, "standard" CFD is used to indicate the hystorical process used to simulate centrifugal compressor stages, i.e. with only the flow-path and blades included into the computational domain, whereas "high fidelity" is used to indicate a complete fidelity reproduction of the geometry and the use of advanced numerical models. All the different aspects between the two approaches will be discussed in details in the following paragraphs.

Figure 5.1 shows the comparison of performance curves between standard CFD, high fidelity CFD and test data for a single stage centrifugal compressor with external impeller diameter of 390 mm., flow coefficient 0.0444 and peripheral Mach number of 0.73. The geometry of the stage, including fillets and leakage flows, is reported in figure 5.2. In particular polytropic efficiency, work coefficient and polytropic head are reported in the performance curves. The black vertical line indicates the stage design flow coefficient. The curves for polytropic efficiency, work coefficient and polytropic head have been derived using respectively equations (5.1), (5.2) and (5.3).

$$\eta_p = \frac{H_{pol}}{\Delta H_0} \tag{5.1}$$

$$\tau = \frac{\Delta H_0}{U^2} \tag{5.2}$$

$$\psi = \tau \cdot \eta_p \tag{5.3}$$

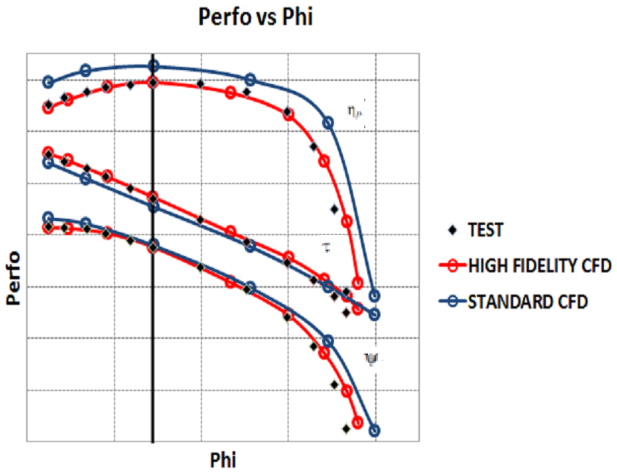

Figure 5.1: Overall stage performance comparison between test and steady CFD for stage flow coefficient 0.0444.

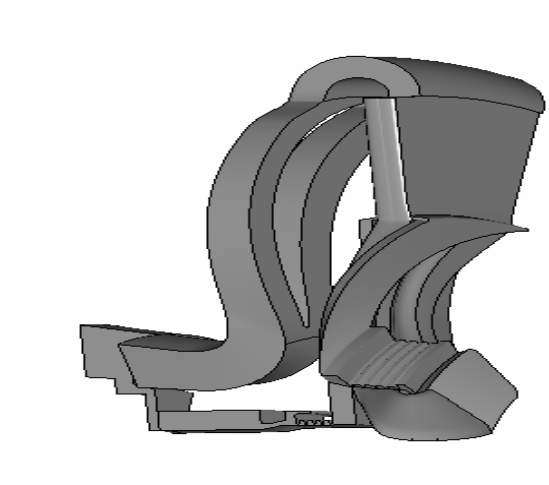

Figure 5.2: Computational domain for stage flow coefficient 0.0444.

In the CFD simulations, total pressure and total temperature were mass averaged. The curves are plotted versus the flow coefficient. All the CFD simulations are steady in time and circumferential averaged profiles are exchanged between blade rows with different

reference frame. As a criterion to assess compressor operating point close to stall flow rate during CFD simulations, runs have been discarded when either the polytropic head curve becomes flat or when onset of numerical instabilities appear. This is not the same as the onset of compressor instabilities like surge or stall, that can be detected during test with dynamic pressure probes. However, numerical instabilities are considered to have a strong connection with non desirable flow phenomena, such as separation or blockage extension.

The improvement in CFD performance prediction accuracy with high fidelity CFD versus standard one is clearly visible. Standard CFD is the one with the highest efficiency as expected and also is the one with the largest stall and choke margins. In fact it is well known that standard CFD tends to under-estimate losses with respect to test data if no additional dissipation terms are used and secondary effects are not modeled properly. Instead, when an high fidelity reproduction of the geometry and advanced numerical schemes are used, CFD predicitons match very well test data.

The stage was tested also in off-design speed; in particular in figure 5.3 are reported also performance curves for peripheal Mach number 0.5 (lower curve) and 0.85 (higher curve).

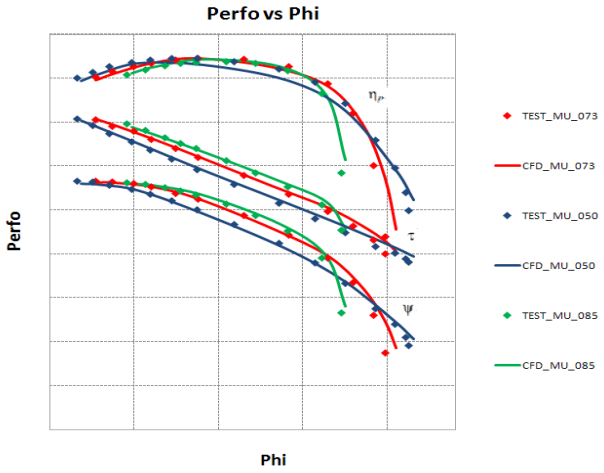

Figure 5.3: Overall stage performance comparison between test and high fidelity CFD for stage flow coefficient 0.0444 at design and off-design speeds.

The comparison clearly suggests that only by using advanced high fidelity CFD accurate numerical predictions are achievable for efficiency, head, and operating margin, otherwise not possible with simplified models.

Figures 5.5 and 5.7 show the same comparison for a very low and very high flow

coefficient stages. In particular the test cases selected are a bi-dimensional stage with flow coefficient 0.0095 and peripheral Mach number 1.0 in over-hung configuration with vaned diffuser and a tri-dimensional stage with flow coefficient 0.1600 and peripheral Mach number 0.85. Computational domains for the two stages are reported respectively in figures 5.4 and 5.6.

Also for these two extreme stages the agreement between test and CFD is very good. The introduction of the new computational models allow to assess centrifugal compressor performance stages with an accuracy not possible before. Moreover, the new methodology has been applied to a large envelope of different flow coefficient and peripheral Mach number stages giving a very good agreement with test data with small deviations across the full spectrum.

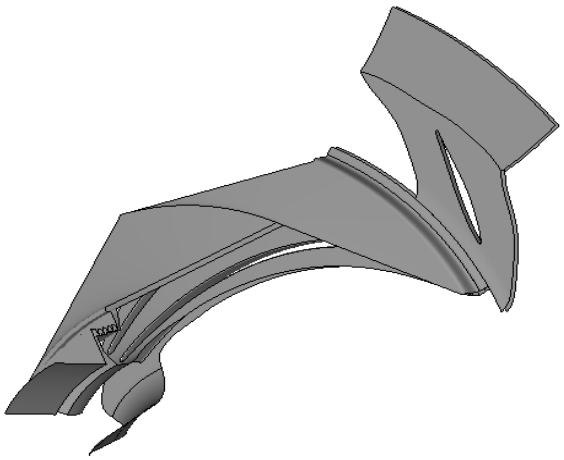

Figure 5.4: Computational domain for stage flow coefficient 0.0095.

In the remained part of this chapter, the influence of all the main actors of the level of CFD accuracy will be described in details.

5.1 Influence of Numerical Schemes

Numerical errors arise from different sources. In particular they can be divided in three main categories:

- Grid resolution

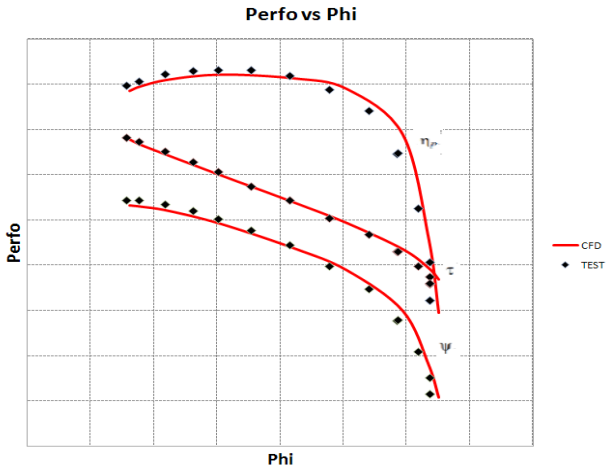

Figure 5.5: Overall stage performance comparison between test and steady CFD for stage flow coefficient 0.0095.

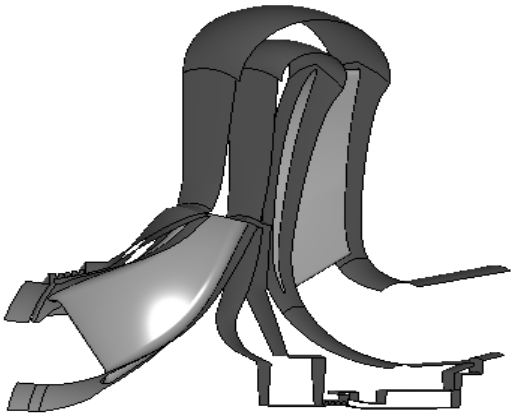

Figure 5.6: Computational domain for stage flow coefficient 0.1600.

- Code stability
- Turbulence modeling

For the first point, with the increasing in computer performance, numerical errors due to inaccurate discretization are becoming nowadays very small. In fact, the accuracy of numerical errors were strongly linked to the limited number of grid points that could be used in the past. Several million of elements for one blade sector are often used for

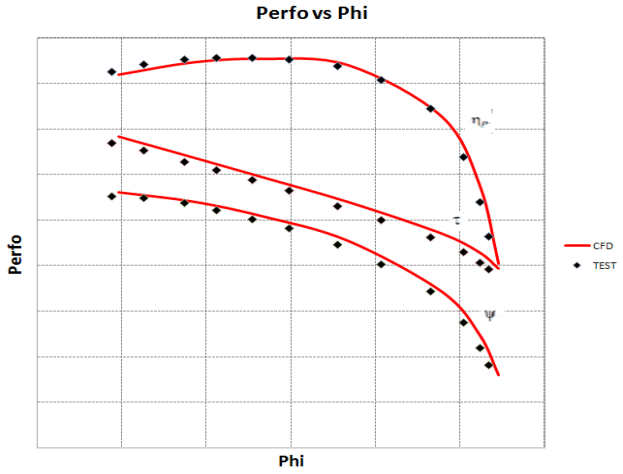

Figure 5.7: Overall stage performance comparison between test and steady CFD for stage flow coefficient 0.1600.

routinely calculations. Many grid independency studies have been performed during this research work and the necessary computational domain discretization to achieve a good numerical resolution has been described in the previous chapter. In fact, as pointed out by Denton in [32], the most common numerical approximation is that the flow properties vary linearly between two grid points and so the error is proportional to the square of the grid spacing times the second derivative of the flow property concerned. A critical area for numerical error in centrifugal compressors is the area downstream the blunt trailing edge of the impeller. Regarding the trailing edge discretization, a C block, instead of the usual O type one, is very useful in the grid topology to avoid dissipating areas and high numerical errors. Details of the grid at the mid-span trailing edge as well as the contours of EGR showing the structure of the two counter-rotating vortices is presented in figure 5.8 for a medium flow coefficient impeller. In fact, the grid at the trailing edge has to be fine enough to resolve the counter rotating vortices and not to show false fluid structures as also shown in [33].

CFD codes are becoming more and more robust. Artificial viscosity has been used extensively in the past to stabilize the numerical algorithms. However, in the common applications of industrial centrifugal compressors, codes robustness limits the use of artificial viscosity to very few tough cases.

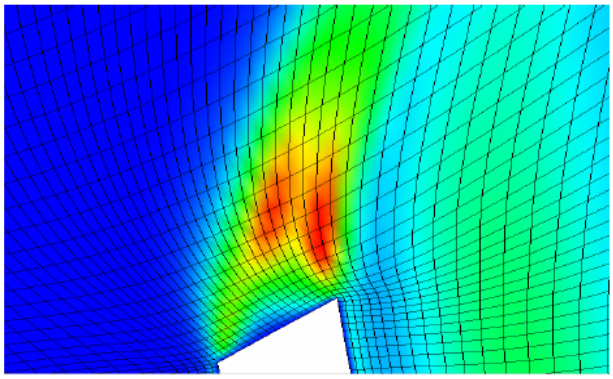

Figure 5.8: Impeller trailing edge grid details and EGR contours.

Turbulent flows occur at high Reynolds numbers, when the inertia of the fluid overwhelms the viscosity of the fluid, causing the laminar flow motions to become unstable. Under these conditions, the flow is characterized by rapid fluctuations in pressure and velocity which are inherently three dimensional and unsteady. Turbulent flow is composed of large eddies that migrate across the flow generating smaller eddies as they go. These smaller eddies in turn generates smaller eddies until they become small enough that their energy is dissipated due to the presence of molecular viscosity. The full influence of the turbulent fluctuations on the mean flow must be modelled. In order to use a larger mesh size and still capture the turbulent flow, the Favre averaged Navier-Stokes equations are used.

For attached fully turbulent boundary layers all the turbulence models are enough accurate to predict flow beahvior. All the considerations are related to RANS models, whereas more refined methodologies like LES and DNS are too expensive to be used in common applications. Bourgeois [8] et al. and Mangani et al. [34] revised accurately the different turbulence models for centrifugal compressor applications. Just few considerations, uncovered in open literature for centrifugal compressors, will be added by the present author. In particular, in the present work both the $\kappa - \omega$ and the SST models have been used. It has been found that the $\kappa - \omega$ is more sensitive to the incoming turbulence length scale than the SST that is so recommended when inlet boundary conditions are not well known. Furthermore, when dealing with high strain flows, e.g. close to choke conditions, the Kato-Launder production limiter variation of both the $\kappa - \omega$ and the SST models has given more accurate agreement with test data. In fact, Kato-Launder modification is an ad-hoc modification of the turbulent production term in the turbulent kinetic energy equation.

The main purpose of the modification is to reduce the tendency that many two equation models have to over-predict the turbulent production in regions with large normal strain, i.e. regions with strong acceleration or deceleration. For separated flows, the eddy viscosity is not allowed to get as large with SST as it does with other $\kappa - \omega$ model (and much less than $\kappa - \epsilon$ models) so that in a flow tending to separate, SST will predict a larger separation region than other models. It has been shown to work well for flows with small separations whereas for flows with larger separations, SST tends to predict separations that may be too large relative to experimental observations. LES calculations might be expected to give better results than RANS calculations for separated regions but several years are still needed before computer power will allow to perform these calculations in standard applications. Furthermore a curvature correction modifier, like the one proposed by Smirnov and Menter [7] has been implemented in the GE in-house code. It has been found that the correction has a clear influence on high flow coefficients stages whereas has negligible effects on low flow coefficient bi-dimensional stages. Also, the effects, are predominanly located at the U-bend of multistage compressors where the accuracy in predicting the separation region is fundamental for the assessment of downstream return channel performance. In fact, analysis of the turbulent flow field showed a clear increased in turbulence production near concave surfaces and decreased production near convex surfaces with connected different loss generation mechanisms.

Finally, transitional flows are often present in many practical cases. Transition refers to the process when a laminar boundary layer becomes unstable and turbulent boundary layer develops. There are two types of transition: natural transition, where inherent instabilities in the boundary layer cause the transition and by-pass transition, where convection and diffusion of turbulence from the free-stream into the boundary layer cause the transition. Most transitions in turbomachinery are by-pass transitions caused by free-stream turbulence and other external disturbances like wakes, vortices and surface defects. Simulating transition in a CFD code accurately is very difficult, sometimes almost impossible for very complex cases. Recent transitional models claim the ability to correctly simulate the effects of transition even if much work still needs to be done on this subject.

5.2 Influence of Boundary Conditions and Gas Model

Inlet and outlet boundary conditions are fundamental to correctly model centrifugal compressor stages. Usually, tangential averaged profiles of total quantities and angles are used at stage inlet section. Total pressure, total temperature and flow angle profiles were applied as inlet conditions. Static pressure profile is applied at the outlet. A great amount of test data is available in the GE Oil&GAS database and accurate boundary conditions are always applied in the CFD runs. Furthermore, recently, a great effort has been put in measuring inlet turbuence conditions. In fact, a wrong estimation of the turbulence level at inlet can lead to an over-production or under-production of turbulent kinetic energy inside the stage with an inaccurate prediction of entropy and at the end losses. Two equations turbulence models require the specification of both turbulence intensity and length scale or some derived quantities. Hot-wire anemometry systems are currently employed at the author's OEM test benches to estimate turbulence level. The incoming turbulence length-scale is often even more difficult to guess than the incoming turbulence level. The best way of guessing a realistic incoming length-scale is to use the geometrical properties of the upstream components. Fortunately the incoming turbulence length-scale is usually not that important for the end results.

Single stages centrifugal compressors are routenely tested with air, carbon dioxide or refrigerant gases. Multistage centrifugal compressors are instead operated with very different gases and operating conditions that can range between light gases like hydrogen and heavy hydrocarbon mixtures and between atmospheric pressure and several hundred bar. In CFD gas models can vary from simple constant properties to real gas algorithms. In many cases (e.g. air at atmospheric inlet pressure), the inaccuracy in using a constant properties gas model is negligible. Challenging applications like carbon dioxide close to critical conditions require instead a real gas properties model to accurately predict the performance of the compressor. In between these two options, a linear γ gas model is often a good compromise between accuracy and execution time. The two main parameters that affects the choice of the gas model are the compressibility factor Z and the isoentropic exponent γ. It has been found that up to few percent of variation inside the compressor for both the parameters, the perfect gas model offers a good prediction of stage performance. For higher variations, e.g. in the order of 5% or more, the inaccuracy tends to be not negligible.

5.3 Influence of Geometry Fidelity Reproduction

A fidelity representation of the geometrical features is a critical factor in CFD accuracy. The main sources of uncertainties in the geometry definition are usually related to:

- Leakage flows modeling
- Fillets
- Leading edge, trailing edge and blade profile shapes
- Hot geometry and tip clearance for open impellers

Regarding the first two points, up to few years ago, the grid generation software packages did not allow to mesh the geometry properly. For the leakge fows modeling, in the next paragraph, a detailed explanation of the implications on CFD accuracy will be presented. For the impeller fillets, it is clear that operating range, especially choke margin, and the amount of work transferred from the impeller to the gas, are related to the fillet radius and shape. Furthermore, a connection between the capability of the impeller to resist at high incidence levels close to the blade tip and the fillet radius in that zone is well established.

Blades profile and, in particular, leading edge shape, is another sources of possible simulation inaccuracies. If the blade shape is often well modeled in the computational domain with a reasonable number of grid points, the leading edge shape is more sensible to possible mismatching between real geometries and simulated ones. In fact, inaccuracies in the stagnation point caption in the virtual simulation can lead to a misleading prediction of boundary layer development on the blade surface. To correctly model the rapid accelerating and decelerating flow in that area a very fine grid is mandatory.

Manufacturing variabilities and uncertanty quantification are being studied in details by Panizza et al [35], [36] and [37] in the same author's OEM and the implications on CFD predictions are explored. It has been shown that the scatter for polytropic efficiency is largest at surge and smallest near peak efficiency, while it is largest near choke for work coefficient. Impeller exit width and angle are critical parameters for all responses at all flow coefficients. However, away from the design point, other parameters gain a considerable influence, such as inlet angles for efficiency towards surge, and impeller eye clearance for work

coefficient, again in the surge region. Again, inlet and outlet fidelity geometrical impeller modeling has been shown to be fundamental for compressors performance quantification.

Finally, tip clearance shape is often not well know in open impellers especially for transonic stages where the running blade overall shape should be estimated by stress analysis in hot conditions. The present work is mainly focused on closed impellers and already detailed implications of these uncertanties on endwall losses and stall margin are present in open literature, mainly for aero-engines applications like in the work from Hah [5].

5.4 Influence of Leakage Flows Modeling

Regarding efficiency, it is well known that CFD without cavities modeling under predicts losses generation due to the lack in capturing main secondary flows effects. Regarding the operating range, it is clear that stall limit is influenced by instability effects on flow angle at impeller exit due to the leakage cavities. In addition to this, the perturbated adverse pressure boundary layer at the impeller inlet shroud cavity re-injection implies a different flow incidence that affects both efficiency and stall margin. At overflow conditions an additional mass flow is recirculating inside the impeller due to the presence of the shroud cavity that implies a shift of the operating conditions of the impeller towards choke conditions. Work coefficient is the least affected by the introduction of cavities modeling.

Cavity modeling plays a fundamental role in the performance prediction. In particular losses associate with leakage flows are relevant and this is expect to increase with lower flow coefficient stages. In fact leakage mass flow scales with impeller pressure ratio and cavity geometry, in particular number of labyrinths, labyrinths clearance and cavity roughness that do not scale with flow coefficient. It is well know that centrifugal compressor stages have the maximum efficiency in the range of medium flow coefficients (0.0444-0.0956). Moving up in flow coefficient stages, profile losses become higher; moving down skin friction losses become predominant. A linear trend can be observed for cavity flow losses moving from the highest flow coefficient stages to the lowest ones. In Figure 5.9 and Figure 5.10 it can be observed the efficiency and work coefficient difference from CFD simulations for the cases with cavities across the full spectrum of flow coefficients and peripheral Mach numbers usually used in practical applications. Performance data are reported to the same conditions at design speed with respect to no cavity cases. Moving to lower flow coefficient impellers,

stage efficiency decreases not only due to the increased dissipation inside the main flow path but also the windage and leakage losses. If, for medium flow coefficient impeller leakage losses are in the order of 2/3%, for a very low one it can reach up to 6/7%.

As stated above also an effect on work coefficient can be associated with the leakage flow, even if quantitatively smaller with respect to the losses increase. In fact compressed hot flow passing through the shroud cavity re-enters before impeller leading edge. Two effects counter-act: the higher mass flow passing through the impeller due to the recirculating forward cavity leakage, forces the impeller to work more on the right side of the characteristic line. Instead the compressed and hotter re-entering leakage flow upstream leading edge goes in the opposite direction. Depending on the stage design and compressor operating point one or the other effect prevails and the work coefficient is affected consequently. Furthermore, the flow re-entering the main flow from the shroud cavity affects the swirl close to the tip impeller and so the amount of work transfered by the impeller to the flow. In the case reported in figure 5.1 very small variation with respect to the model without cavities included can be seen all across the performance line.

Effects of leakage flows are also very important in off-design speeds when standard CFD is not even able to match performance on a delta basis. In fact, as it can be noted in figure 5.3, CFD is able to match with a very good accuracy not only design speed performance curves but also off-design speed curves. This was possible only by including leakge flows into the model since the mass flow through the front and back sides cavity changes accordingly with different head coeficient. Without including leakage flows into the model, only the effect of off-design blading losses are captured leading to under or over prediction of efficiency decrement with respect to design speed.

In figure 5.11 is shown the comparison of leakage flow amount between CFD and correlations at different operating conditions for the stage flow coefficient 0.0444 described before. Correlations used for assessing the leakage flow amount are derived from the original work of Daily e Nece and available in open literature. The agreement between CFD and 1D correlations is good expecially at design and close to choke condition. Close to stall the CFD is able to better segregate the 3D effects and the leakage amount increases sensibly. For the stages at lowest flow coefficients the width of the cavities become of the same order of the main flow-path and combined with the higher pressure ratio achieved translates in larger leakage flow that can reach several percentage points with respect to the main flow.

Finally, the correct modeling of the shape and position of the area close to the

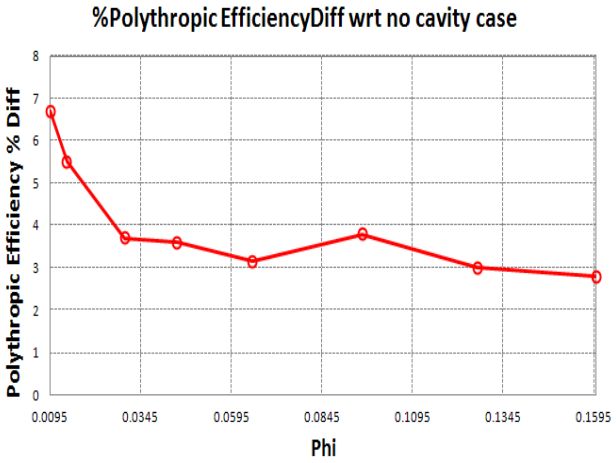

Figure 5.9: Leakage flows efficiency decrement across the full range of flow coefficient stages.

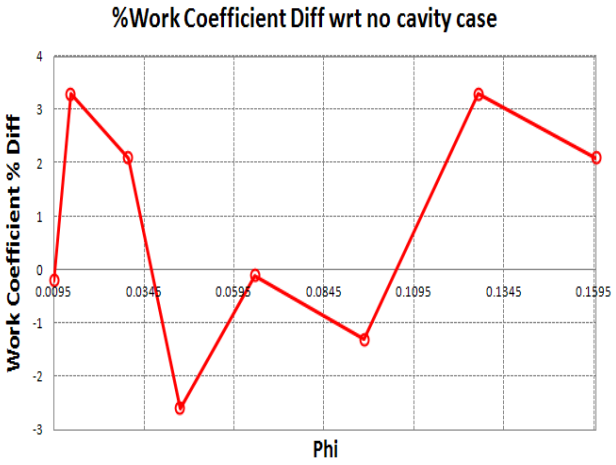

Figure 5.10: Leakage flows work coefficient effect with respect to no cavity flows across the full range of flow coefficient stages.

interface between the leakage flow and the main flow-path is fundamental in order to release the flow inside the compressor with the appropriate turbulent kinetic energy that will affect the boundary layer thickness in an area of adverse pressure gradient of the flow that is prone to separation.

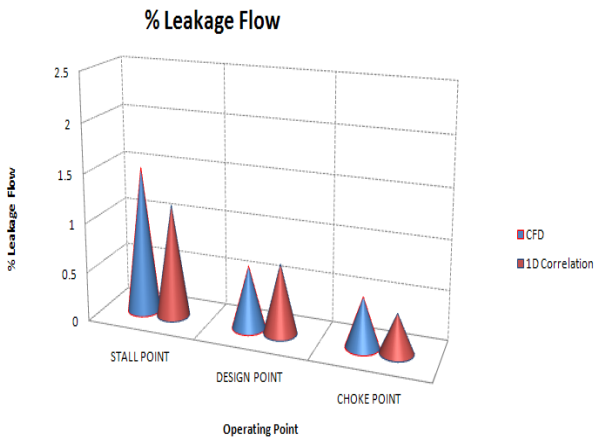

Figure 5.11: Comparison of leakage flow amount between CFD and correlations at different operating conditions for the stage flow coefficient 0.0444.

5.5 Influence of Surface Roughness

Surface roughness influence on predicatability accuracy can vary largely based on compressor main source of losses and Reynolds number. For an high flow coefficient tri-dimensional impeller the effect of skin friction losses is much lower than a bi-dimensional low coefficient stage. Moreover, depending on stage operating Reynolds number, viscous terms can become a large source of losses also for high inlet volumetric flow stages. The effect of surface roughness in CFD modeling is clearly related to the boundary layer thickness. A detailed sensitivity analysis, both experimental and numerical, at different surface roughness and for different stage type has been conducted during this research projects. A transition Reynolds number and stage flow coefficient have been found at which the surfaces can not be considered anymore hydrodinamicaly smooth. In fact, for a medium flow coefficient stage at atmospheric inlet pressure, the effect on performance of the roughness model can be neglected; instead for a low coefficient stage at several hundreds bar inlet pressure the losses are under-predicted if the roughness model is not included in the numerical setup. The effect of roughness model on the work transfered from the impeller to the fluid it has been found to be lower than the one on efficiency. Another source of uncertainty in using the roughness model is the implementation of the model itself in all the CFD codes; in fact the value to specify for surface roughness is not the real roughness but the sand grain roughness.

In open literature different relations can be found between sand grain roughness and real roughness ranging from a value of 2 up to 10. Many validation cases have been run to assess this information in the present study.

Surface roughness is also very important to correctly assess the stall margin into the diffuser. It is well know that very low roughness value could avoid the transition from laminar to turbulent flow in some cases and so to limit left operating range.

5.6 Multistage Effects

All the numerical and discretization uncertainties described before become even more critical when dealing with multi-stage turbomachinery simulations. In fact, it is sufficient that one of the stages of a multistage centrifugal compressor is not correctly predicted in terms of performance curves in the CFD simulation, that all the following stages will work at a different operating point from which they have been designed. In other words, it is sufficient than one stage is not correctly modeled that a mismatching will derive. Not only overall single stage performance needs to be correcty evaluated but also released flow profiles at the outlet of each stage needs to be faithfuly reproduced numerically to not affect the behavior of following stages. Furthermore, in multistage smulations also additional features like balance drum leakages, inter-phase leakages, shunt holes and so on, need to be modeled in order to assess overall compressor performance properly.

Figure 5.12 shows the CFD computational domain of a recycling wheel for an ammonia process. The compressor stacking is composed by two sections with inlet and outlet scrolls for each section. The last stage of the first section is connected to the recycling wheel in a back-to-back configuration. The computational model is made by the recycling wheel itself, the inlet and outlet scrolls and the last stage of the first section. Furthermore, all the leakage flows for both the impellers as well as the end drum have been modeled. Details of the back-to-back configuration are shown in figure 5.13.

Aim of the study was to predict the performance of the recycling wheel. This impeller is critical for the process since it sets the pressure at the exit and so the overall process conditions. Figure 5.14 shows the comparison between predicted performance from CFD and test results: the agreement is excellent. As expected the agreement was possible only by fidelity reproducing the computational model. Furthermore, it is mandatory to model the leakage flow passing through the end drum, as shown in figure 5.15 to predict

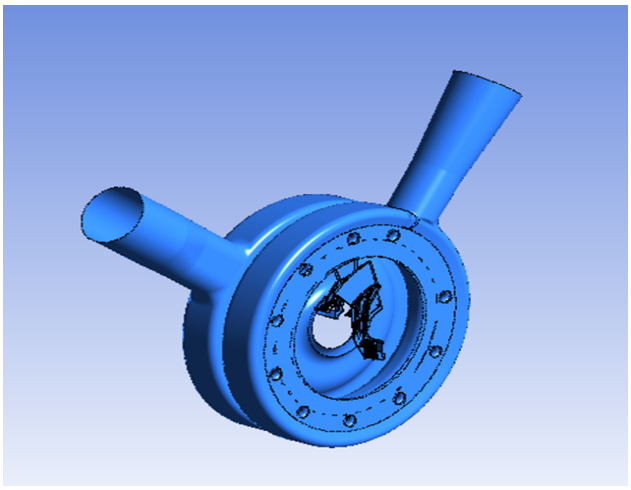

Figure 5.12: Computational domain for a reycling wheel in an ammonia process.

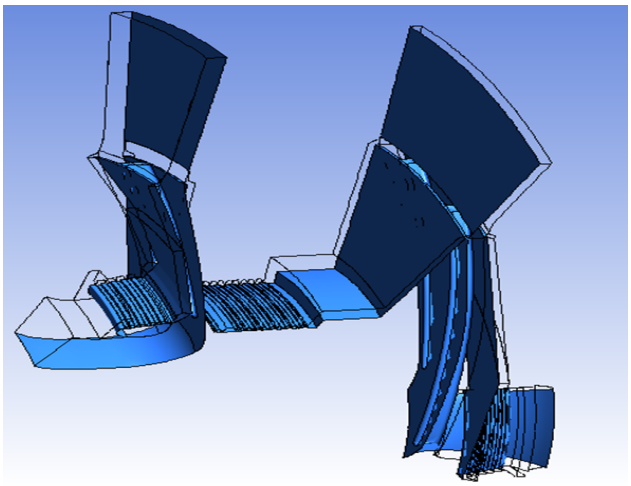

Figure 5.13: Details of the back-to-back configuration.

not only impeller performance but also diffuser and outlet scroll flow profiles and in general overall losses as it will be shown later.

One of the most critical applications in the OIL&GAS market are the compressors for LNG process. An example is reported in figure 5.16. The compressor is made by 5 stages and it is divided into four sections with one inlet plenum and three side-streams. Operating conditions go from several degrees Cesius below zero and atmospheric pressure at inlet up to several tens of bar and degrees Celsius at the outlet. In the computational model, to reduce

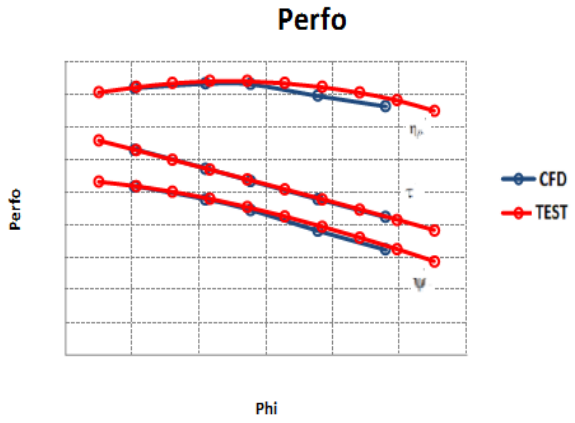

Figure 5.14: Comparison between predicted performance from CFD and test results for a reycling wheel in an ammonia process.

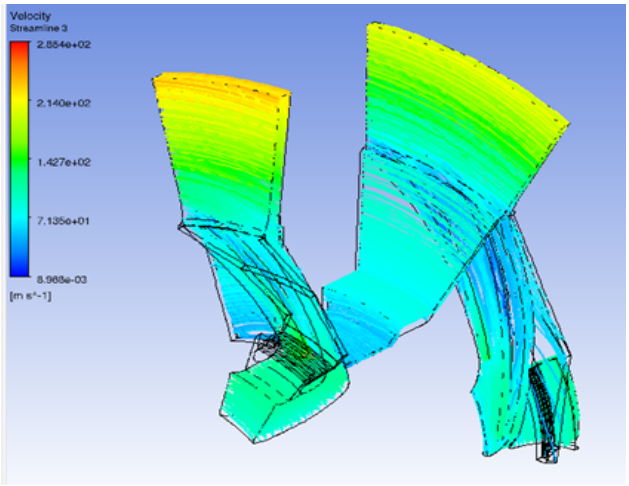

Figure 5.15: Streamlines for the back-to-back system coloured by velocity.

the size, the stationary components were not included like in the previous one but all the inlet boundary conditions for the stages were extracted from previous CFD computations of all the stationary components. A real gas model for propane was used. The balancing line, connecting the outlet with the inlet, was taken into account in the model with a source term approach. As per API-617, the different sections can be tested separately with some acceptance on flow deviations. In figure 5.17 is reported the performance curves predicted

by CFD and measured in the string test for the first section that is the most critical. The other sections are not reported here for semplicity but the overall considerations are still valid. The top graph shows the polythropic head in meters, isntead the bottom one the polythropic efficiency. Both are plotted versus inlet volumetric flow. The stages are high Mach, high capacity tri-dimensional ones. The agreemnt is very good between test and CFD. Furthermore the operating range is correctly matched ensuring a safe opeartion of the compressor on field.

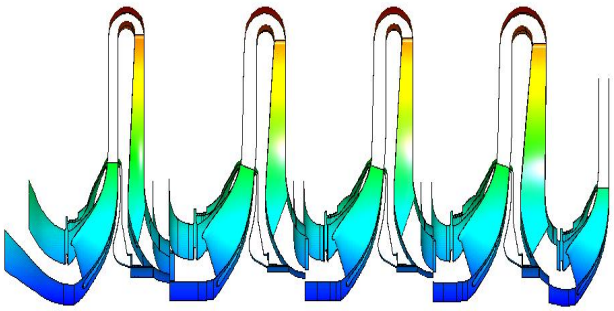

Figure 5.16: Multistage centrifugal compressor for LNG application.

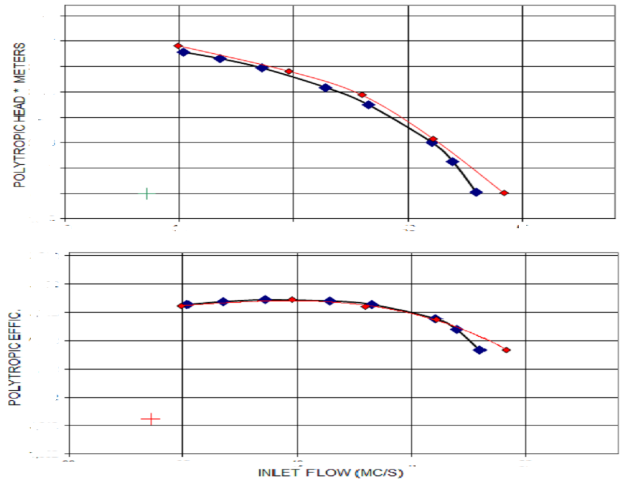

Figure 5.17: Comparison between predicted performance from CFD and test results for section 1.

5.7 Influence of Unsteady Flows

On one hand, when dealing with unsteady flows, fluid dynamics computations require long solution times and therefore require huge computing and human resources. On the other hand, steady computations are not sufficient to fully understand phenomena like blade row interaction, stall, distortion and hot streak migration that are inherently unsteady.

Unsteady turbomachinery simulations require the modeling of a common pitch between adjacent blade rows to apply instantaneous periodic conditions. However, to avoid resonance effects commonly rotors and stators have different blade counts; for all the cases where no common pitch can be found between rotor and stator, a full annulus simulation is necessary. This requires computational and memory efforts not applicable in most of the industrial cases. Using the phase-lag method, temporal periodicity due to adjacent blade interaction can be modeled with single passage. Phase-lag methodology can be applied for periodic blade rows, whereas a ful annulus model is required when no axis-symmetric geometry are present.

Compressor operating left limit is in general the one with the lowest prediction accuracy. This is connected to the increment in unsteadiness as long as the compressor operating point moves towards surge. Steady computations are known to be weak in this effort and transient analysis is required. This is particularly true when sudden and strong phenomena happens like in impeller or diffuser stall. Steady computations are accurate enough to predict overall performance curves but they lack in capturing rotating stall phenomena. In figure 5.18 is shown the computational model for an over-hung impeller plus vaned diffuser. It is well know that mixing plane approach under-estimates separated shroud region at diffuser inlet that is a relevant feature in surge margin assessment on this low flow coefficient, high Mach stage. Anyhow, there is also experimental evidence that stability is affected by leakage flows, especially at shroud side cavity where the out coming flow affects the angle profile: to this intent, unsteady simulations with cavity flows modeling are able to closer match the experimental data with respect to steady simulations without.

Figure 5.19 shows the performance comparison for the stage between steady CFD, unsteady CFD and test data. Looking at the test data it is clear that strong unsteadiness happens suddenly moving towards left operating limit. Since the work transfered from the impeller to the flow continues to increase, the stall seems happening inside the diffuser. Furthermore since dynamic pulsations of static pressure are stronger at section 40, i.e.

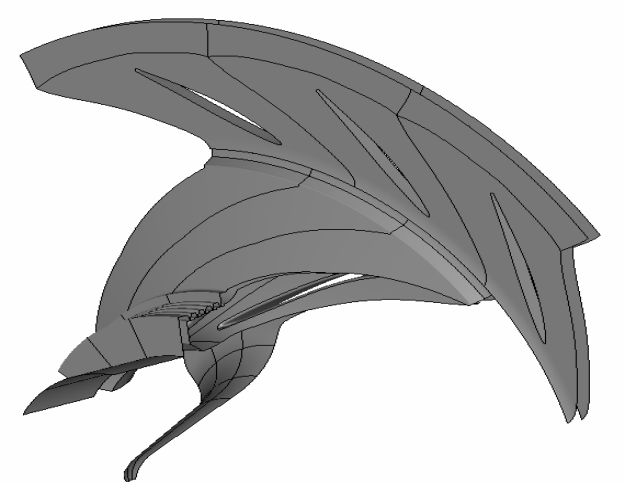

Figure 5.18: Computational domain for an over-hung impeller plus vaned diffuser.

diffuser outlet than other locations and the frequency of sub-syncronous vibrations are the ones common for stationary components, the conclusion is that some blades into the diffuser are too loaded and so stalled. Steady CFD is not able to model rotating stall; an indication of aerodynaic instabilities comes looking at the convergence but the effect seems to be mild compared to the real phenomena. instead unsteady CFD is able to predict with greater accuracy the sudden drop in stage efficiency due to the strong unsteadiness inside the diffuser. Furthermore, an FFT of the signal from usnteady CFD coming from virtual probes inside the computational domain showed a comparable frequency for the phenomena with test data.

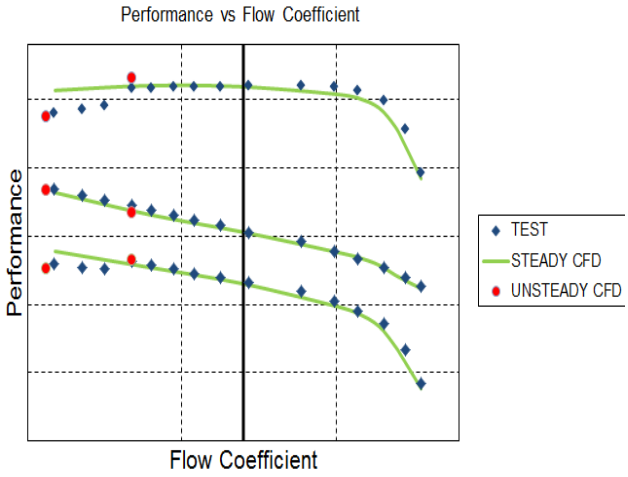

Figure 5.19: Steady and unsteady CFD predictions and test data for an over-hung impeller plus vaned diffuser.

Chapter 6

Flow Analysis

In this chapter the flow field inside the different components of a centrifugal compressor will be analysed in details with the aim to understand and explain aerodynamics phenomena not fully captured before.

6.1 Impeller Flow

Figure 6.1, 6.2 and 6.3 show the 2D maps at section 20 for total pressure from FRAPP, high fidelity CFD (with leakage flows model included) and standard CFD (without cavity flows model included) at design mass flow rate, close to surge and close to choke. The test case reported here is a tri-dimensional impeller, single stage (impeller, vaneless diffuser and return channel) at medium flow coefficient for general purposes applications already described in figure 5.2.

The measurement plane is at section 20, i.e. downstream of the impeller trailing edge, where the FRAPP measurements were taken. The maps refer to two blade pitches An highly non uniform flow field is presented from experimental data with huge defects at some positions close to the hub and shroud surfaces. The region of highest pressure is concentrated around mid-span. The pitch value equal to 1 corresponds to the blade suction side. The impeller is rotating from right to left. Profiles from FRAPP are time averaged. Total pressure is normalized by the difference between maximum and minimum value at the measurement plane.

The high fidelity CFD is in very good agreement both qualitatively and quantitatively with FRAPP data; instead at some locations, standard CFD gives misleading results.

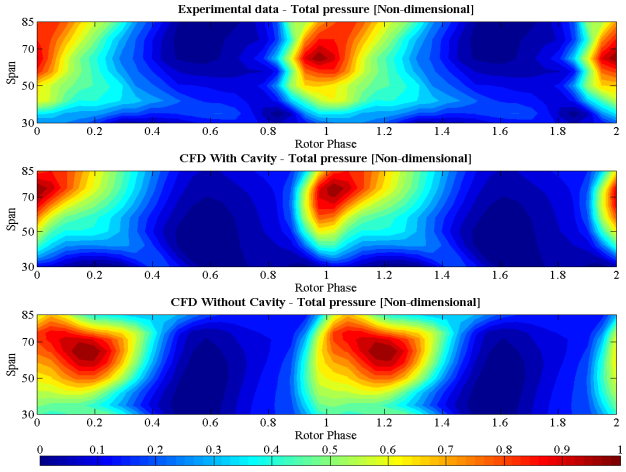

Figure 6.1: FRAPP and CFD total pressure 2D map at section 20 comparison at design flow rate.

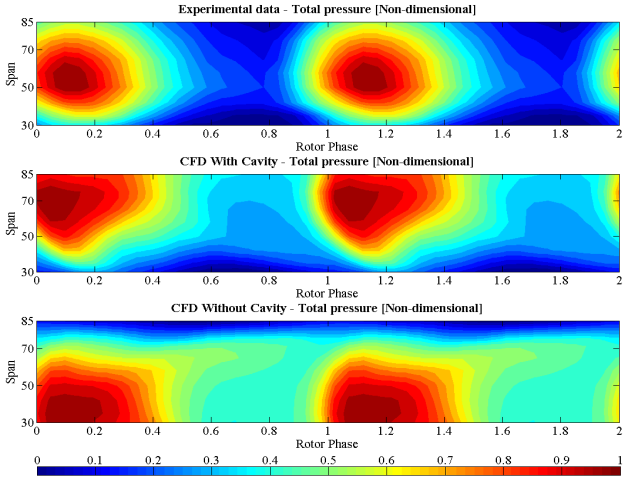

Figure 6.2: FRAPP and CFD total pressure 2D map at section 20 comparison close to surge.

The capability to correctly reproduce the flow features at the impeller trailing edge with CFD is fundamental for the design of diffuser and downstream stationary components optimization. In fact the correct design and optimization of downstream stationary components requires an accurate modeling of flow phenomena at impeller trailing edge.

The absolute total pressure maps present a highly nonuniform pattern both along the spanwise and tangential directions for both FRAPP and high fidelity CFD. The high

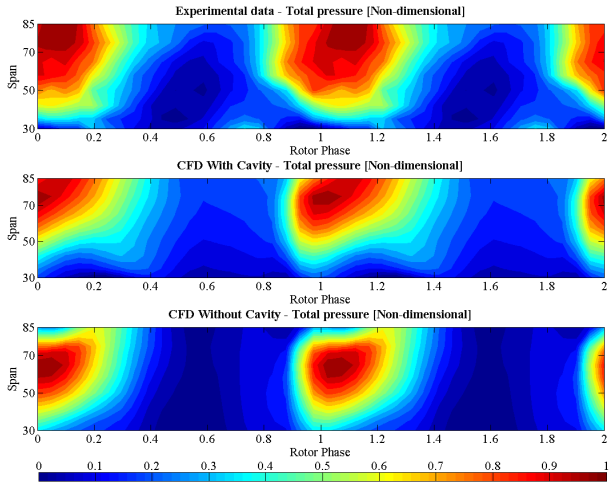

Figure 6.3: FRAPP and CFD total pressure 2D map at section 20 comparison close to choke.

total pressure zone is contoured by a low pressure zone and a considerable defect close to both hub and shroud. In particular, both the FRAPP and CFD total pressure maps present a reduced total pressure zone in the region identified as the wake zone (defined by high tangential flow). The low total pressure region at the hub has historically been one of the most difficult areas for CFD to reproduce. This is mainly due to the high tangential flow re-entering from the cavity at the hub. It should be noted here that all the previous analysis in open literature did not show same agreement. The high pressure zone is located close to shroud side at high and design flow coefficients and moves towards mid-span at lower ones. Moving away from design point the high pressure zone spreads and the non uniform pattern is more pronounced in the circumferential direction.

Slightly higher differences between experimental data and high fidelity CFD with cavities modeling can be found quantitatively at close to stall and choke operating conditions where unsteady effects are predominant.

Figures 6.4, 6.5 and 6.6 show the 2D maps at section 20 for YAW angle. The yaw angle is calculated as per equation (6.1).

$$yaw = tan^{-1}\frac{V_\theta}{V_M} \tag{6.1}$$

Flow angles are plotted with respect to the radial direction and are positive if the tangential velocity has same sign than the impeller peripheral velocity. More tangential flow

angle is associated with greater values.

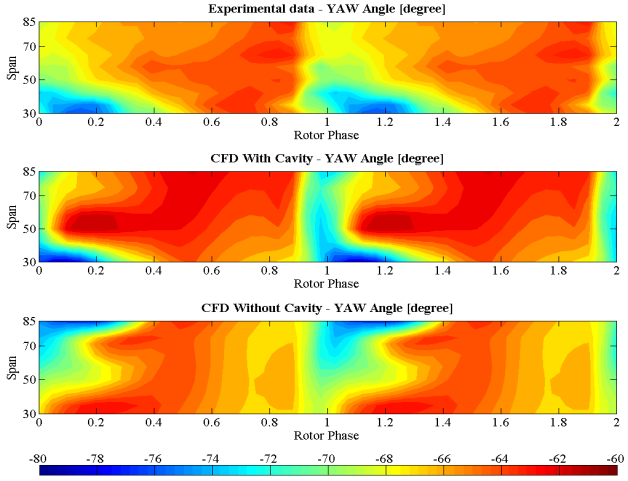

Figure 6.4: FRAPP and CFD YAW angle 2D map at section 20 comparison at design flow rate.

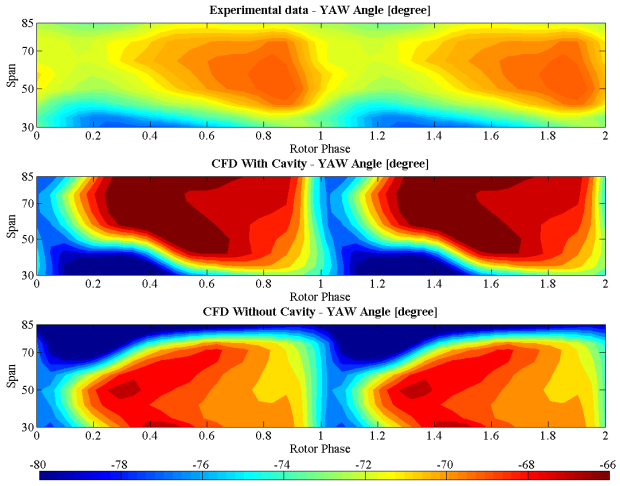

Figure 6.5: FRAPP and CFD YAW angle 2D map at section 20 comparison close to surge.

In the yaw angle maps a very similar flow distribution between FRAPP and high fidelity CFD can also be observed. In fact, both maps have a more tangential flow region in the suction side-shroud corner than in the main core region of the flow. This distribution corresponds to the classical two-zones of jet and wake model. The wake formation inside the impeller is interesting due to its strong interaction with loss generation. In closed impellers

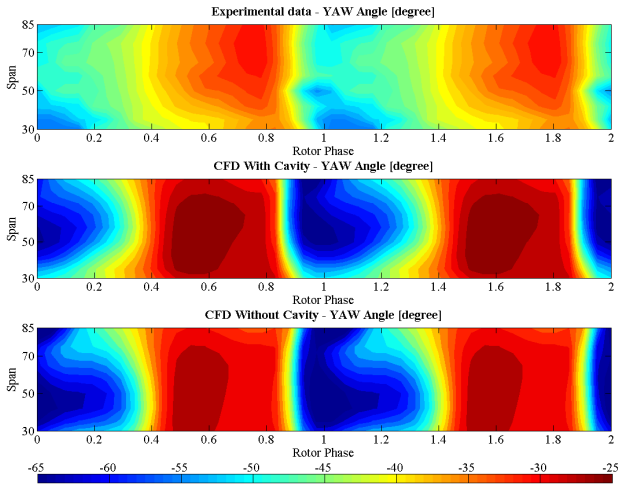

Figure 6.6: FRAPP and CFD YAW angle 2D map at section 20 comparison close to choke.

the wake is usually positioned close to the center of the channel. The flow angle difference between the jet and wake zones has implications on velocity triangles at the impeller exit. In particular the wake region is characterized, in the absolute reference of frame, by a high tangential, high momentum flow that concentrates at the suction surface-shroud side in agreement with [5], [38] and [39]. In fact in centrifugal compressor impellers a strong secondary flow region develops through the passage and this low momentum flow region is concentrated in the shroud surface suction corner whereas the flow is well energized near the hub. This secondary flow detaches from the suction surface at the beginning of the back-swept zone and moves away from the wall. The low momentum flow is responsible for the highest losses in the impeller. This affects not only the impeller flow field but also the angle distribution at the exit of the impeller. The absolute flow angle at the diffuser inlet will be more tangential near the shroud and more radial near the hub region, leading to a complex flow evolution in the diffuser channel. In fact, this non-uniformity in the yaw angle field at the impeller outlet originates two counter-rotating vortical structures in the diffuser that reduce the component efficiency. Moreover, the secondary flow region is due not only to possible separated regions in the impeller, especially close to stall conditions, but also to skewed boundary layers and secondary flows. Both CFD and FRAPP give a more developed and dissipative pattern close to the tip as a result of the strongest flow phenomena occurring in the impeller region. Maximum difference between jet and wake zones is about 30° close to choke operating point. High tangential flow zones are associated

with more dissipative flow behavior and higher turbulent kinetic energy. Higher tangential flow region can be found, as expected, close to stall point. Turbulent kinetic energy (TKE) can be derived from both FRAPP and CFD and can be linked to the flow structures shown before: the pattern reveales a strip along the blade span and two regions of higher turbulent kinetic energy are reported close to the endwalls with a peak value near to the hub as shown also by [4]. Both regions are the result of the interaction between the impeller wake and the strong dissipative secondary flows regions developed at the impeller trailing edge.

Figure 6.7 and Figure 6.8 shows the comparison at the measurements location of the tangential averaged span-wise profiles respectively for yaw angle and total pressure for FRAPP data and both standard and high fidelity CFD simulations. The test case the figures are referring about is still a tri-dimensional impeller, single stage (impeller, vaneless diffuser and return channel) at high flow coefficient and high peripheral Mach number for LNG applications shown in figure 4.1.

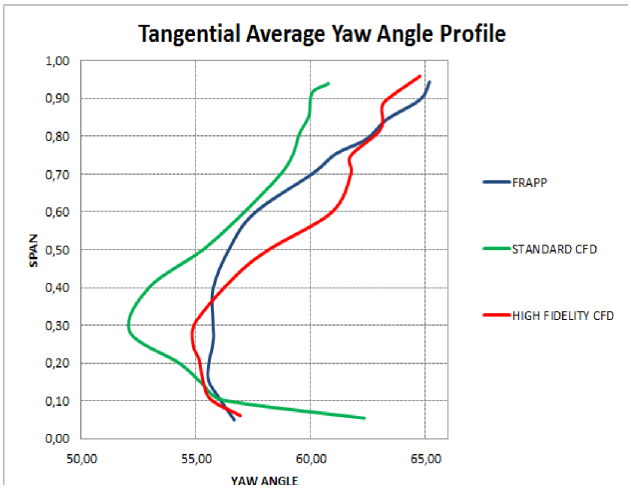

Figure 6.7: Yaw angle comparison between FRAPP and different CFD approaches at impeller exit.

An highly non uniform flow field is presented from experimental data with huge defects at some positions close to the hub and shroud surfaces. The region of highest pressure is concentrated around mid-span. The impact of the high fidelity approach with full cavities modeled on impeller exit profile is strong. In fact, the standard CFD approach has been found historically to be weak in capturing correctly these profiles.

At design point the flow direction in the hub cavity is from return channel trailing

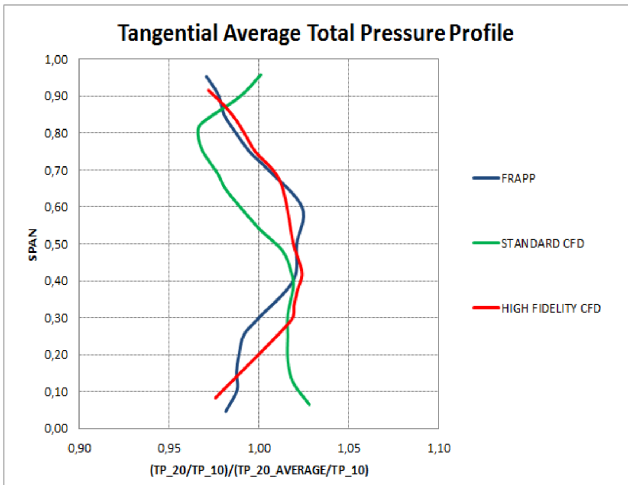

Figure 6.8: Total pressure comparison between FRAPP and different CFD approaches at impeller exit.

edge towards impeller trailing edge due to the static pressure recovery in the stationary parts being higher than the pressure losses associated with skin friction. High fidelity model with full cavities meshed is able to capture the total pressure profile close both ot hub and shroud sides. In the area close to the non-matching interfaces between impeller trailing edge and both shroud and hub cavities, a strong area of recirculating flow develops. Reverse flow forms across the interface that is well captured by the numerical model. In fact, for the shroud cavity, the effect of the rotating blades is counter-acted by the recirculating flow in the cavity. The impeller pushes the flow inside the cavity but the presence of labyrinths seals mitigate the amount of flow passing through that recirculates close to the impeller trailing edge determining the shroud defect shown in the total pressure profile. Also the effect of the hub cavity on total pressure defect profile at mixing region is clearly visible. The leakge fow coming from the return channel at very high swirl mixes wth the radial flow exiting from the impeller creating a recirculation area responsible of the low pressure close to the wall.

Aerodynamic parameters in the cavities are almost constant due to the axis-symmetry of the geometry except near the interfaces close to the impeller trailing edge where a distorted pressure distribution influences the fluid flow uniformity. With full cavities meshed also tangential profiles of flow at interface can be correctly captured. Figures 6.9, 6.10, 6.11, 6.12 and 6.13 show the average tangential profiles of yaw angle and total pressure and the tangential profiles of total pressure at 10%, 50% and 90%. Close to the wall

locations, the effect of leakages is expected to have a stronger infuence on the flow profiles. The tangential direction refers to two blade pitches and the angle is plotted with respect to the radial direction. The pitch value equal to 1 corresponds to the blade suction side. The impeller is rotating from right to left. The simulated operating point is the design one of the compressor stage descrived previously and the profiles are plotted at section 20. The agreement is very good with all the hills and valleys captured along the tangential direction. It was also found that fillets modeling plays a non negligible role in capturing the tangential profiles. Combined fillets and cavities accurate meshing was possible only with non matching interfaces especially at the trailing edge of the impeller due to the combined high curvature of the flow-path and interaction of fillets with blunt trailing edge. Also, due to the loss generation near the wall regions, the total pressure and its amplitude of fluctuation due to the blade passing are lower in the shroud and hub regions than at the mid-span. Generally CFD is more sensitive to pressure fluctuations than experimental data.

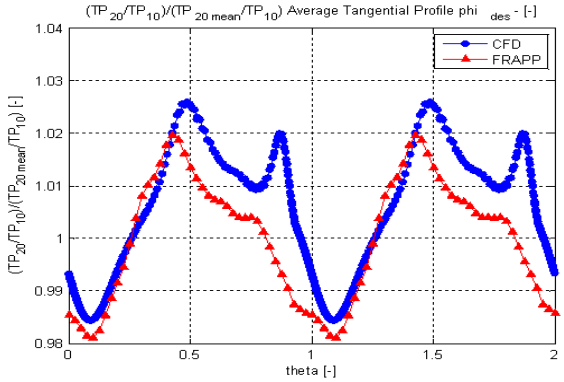

Figure 6.9: Average tangential total pressure profile comparison between FRAPP and high fidelity CFD.

For the same test case, also tangential averaged profiles of YAW angle at off-design points, i.e. close to stall and close to choke are presented in figures 6.14 and 6.15.

CFD show a tendency to slightly under-predict the spread of the quantity across the span at off-design conditions even if the average value is in good agreement with test data. This is in agreement with what can be expected from a steady simulation; in fact, the time averaged of the main quantities tends to smooth out strong and sudden phenomena. In fact, close to stall and close to choke unsteadiness become predominant and in particular close to endwalls where the tri-dimensional effects are higher. However, the agreement on

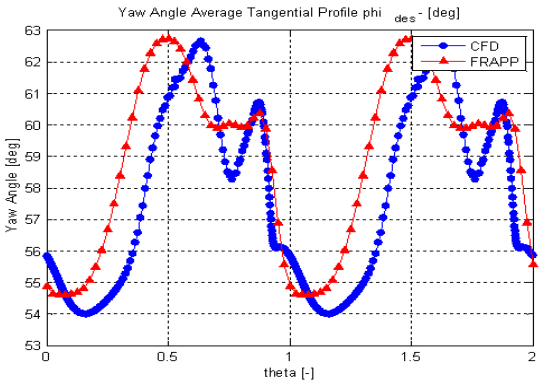

Figure 6.10: Average tangential yaw angle profile comparison between FRAPP and high fidelity CFD.

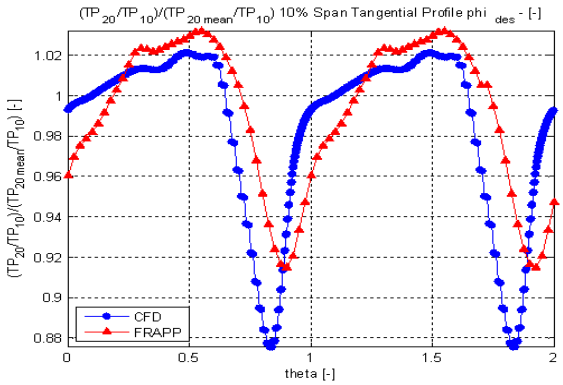

Figure 6.11: Tangential total pressure profile comparison between FRAPP and high fidelity CFD at 10% of the span.

average vaues is very good and overall performance can be then correcty predicted.

6.2 Diffuser Flow

Centrifugal compressors are very difficult to simulate using CFD due to extremely high curvature. This is particularly true for stationary components; standard CFD is historically weak in capturing the correct flow features in downstream stationary components.

In figures 6.16, 6.17 and 6.18 respectively the non dimensional values of total pressure, yaw angle and non dimensional static pressure at section 40 are reported , i.e. diffuser outlet, for both high fidelity CFD and standard CFD. The test case is the one

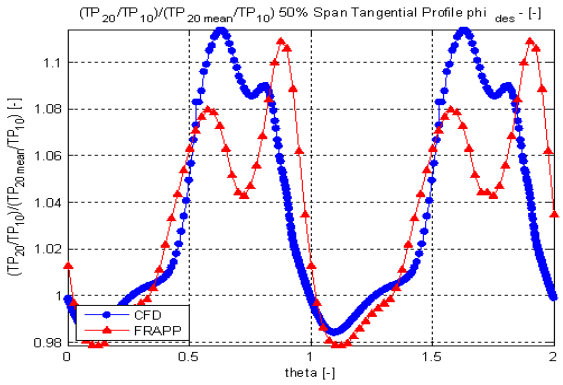

Figure 6.12: Tangential total pressure profile comparison between FRAPP and high fidelity CFD at 50% of the span.

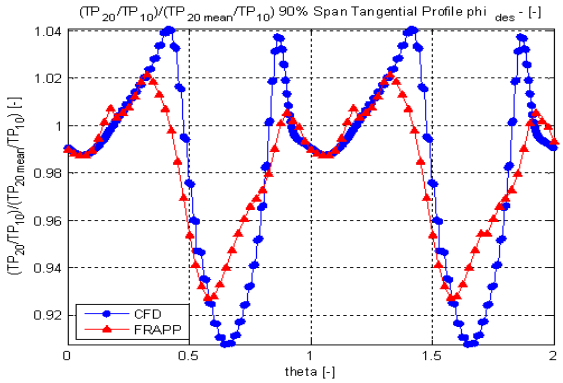

Figure 6.13: Tangential total pressure profile comparison between FRAPP and high fidelity CFD at 90% of the span.

described in figure 4.1.

The aerodynamic behavior of the diffuser is strongly dependent by the leakage flows and can be understood properly only if the modeling of shroud and hub cavities are included in the computational domain. The amount of flow passing through the cavities depends, for a certain geometry, on the pressure ratio delivered by the impeller for the shroud leakage and by the combined effects of pressure recovery and total pressure losses of downstream stationary components for the hub one. Moving from design operating point towards left and right limit the amount of flow through both the cavities tends to increase and decrease respectively. Furthermore in deep choke conditions the direction of the flow in the hub cavity can reverse, i.e. going from impeller to the return channel.

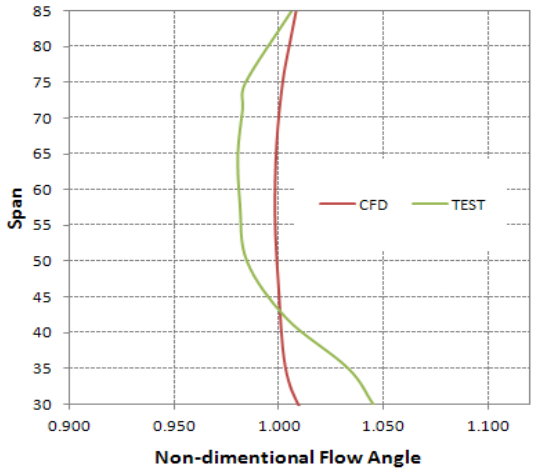

Figure 6.14: FRAPP and CFD tangential averaged yaw angle at section 20 comparison close to surge.

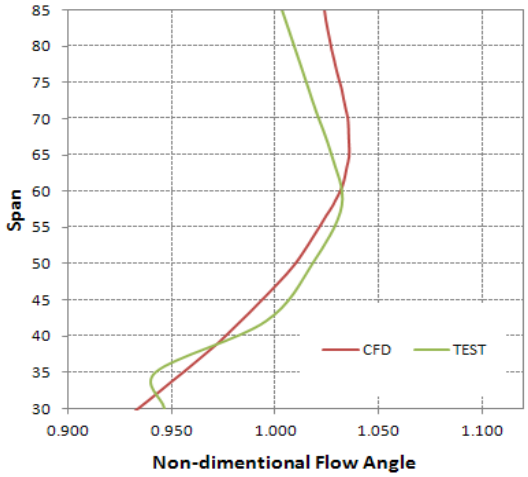

Figure 6.15: FRAPP and CFD tangential averaged yaw angle at section 20 comparison close to choke.

Figures 6.19, 6.20 and 6.21 show the contours plots of meridional velocity inside the diffuser with super-imposed the flow streamlines respectively close to surge operating limit, at design point and close to choke operating points.

First thing to note is the absence, for the high fidelity CFD, of the low momentum zone close to shroud side at the end of the diffuser that has been shown in all previous computations with standard CFD. From the streamlines pattern, it is easy to understand

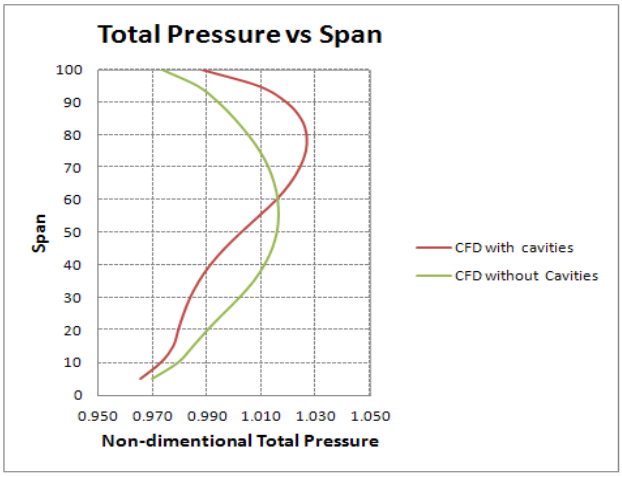

Figure 6.16: Non dimensional total pressure profiles at section 40 at design flow rate.

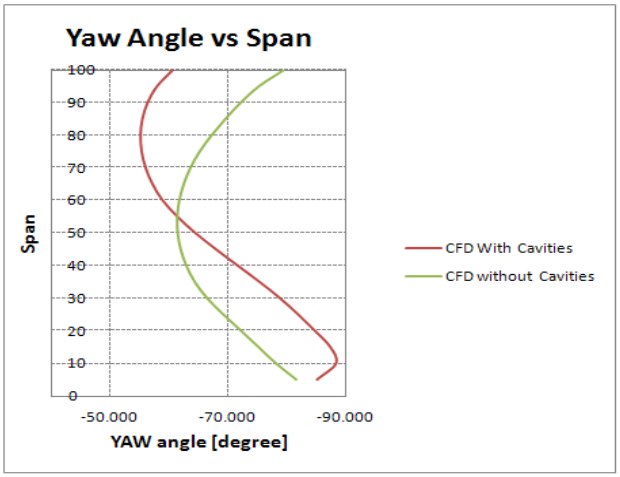

Figure 6.17: Yaw angle profiles at section 40 at design flow rate.

that the high swirling flow coming back into the domain from the hub cavity, pushes the main flow towards the shroud side. This affects also the flow behavior downstream where a region of low momentum flow develops close to the diffuser hub due to the mixing of cavity flow with main-stream.

Close to surge condition, the low momentum zone due to the mixing of the flow re-entering from the hub cavity increases significantly along the hub side and continues downstream up to the diffuser end. Without modeling cavity leakage domains, this phe-

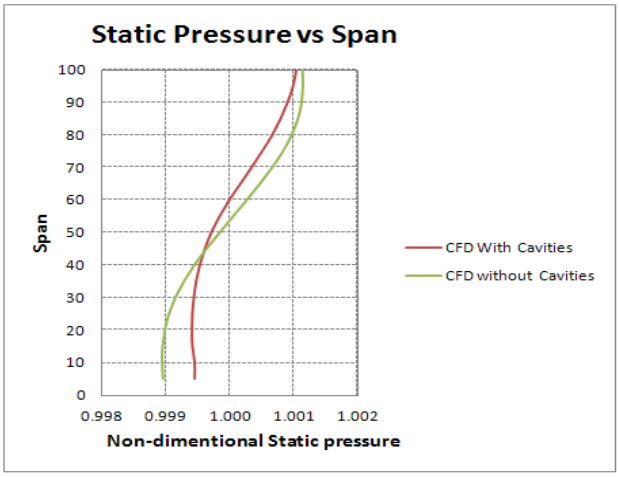

Figure 6.18: Non dimensional static pressure profiles at section 40 at design flow rate.

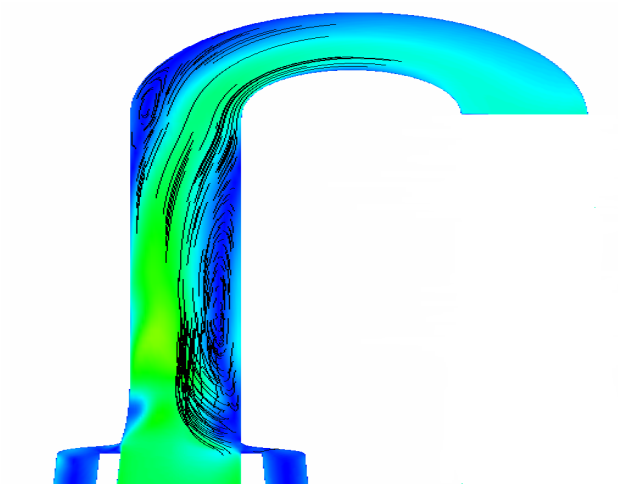

Figure 6.19: Meridional velocity contours inside the diffuser close to surge operating limit.

nomenon was explained in the past, with an apparent switch of diffuser low momentum area from shroud to hub at lower flow operating points as shown by Sorokes et al. [9]. Including cavity domains into the model the picture that comes out looks different; in particular the flow on the shroud side close to the diffuser end tends to separate due to the diffusion inside the diffuser and the higher tangential flow at the end of the impeller. The last phenomenon is obviously correlated to diffuser/impeller ratio and pinch amount.

Close to choke operating limit the influence of both leakage flows is much smaller

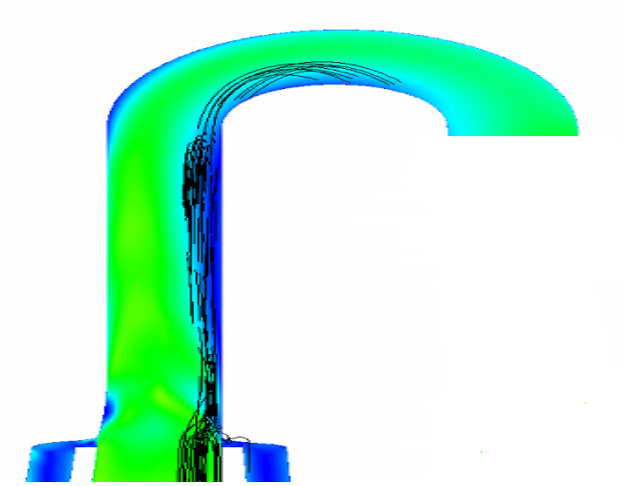

Figure 6.20: Meridional velocity contours inside the diffuser at design operating point.

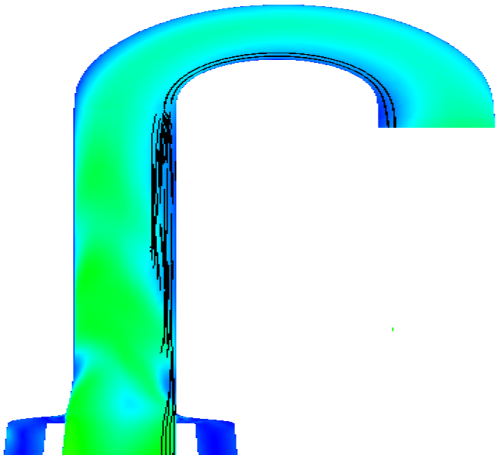

Figure 6.21: Meridional velocity contours inside the diffuser close to choke operating limit.

and translates in lower separated regions both close to shroud and hub endwalls.

Figure 6.22 and 6.23 show the CFD profiles of yaw angle at diffuser exit and the comparison of average value between high fidelity CFD and test respectively close to surge, design and close to choke operating conditions. Yaw angle values are negative and with respect to the radial direction that means more tangential flow towards the left.

The agreement between test and CFD is very good as shown. The average yaw angle becomes more tangential moving from choke to surge as expected. The effects of cavity

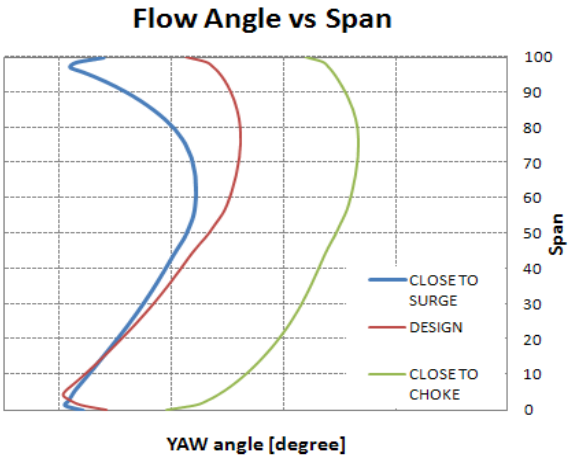

Figure 6.22: Yaw angle profiles at diffuser exit from CFD close to surge, design and close to choke operating conditions.

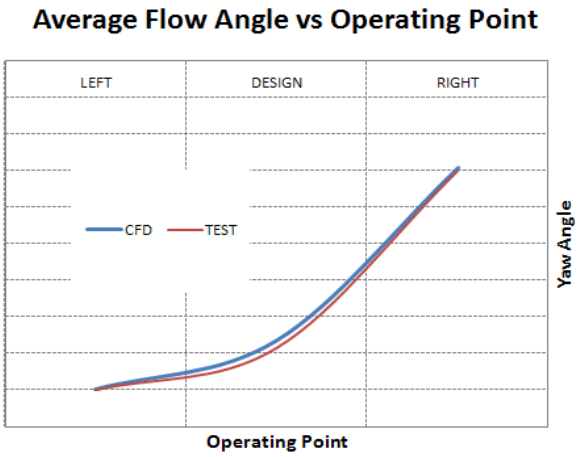

Figure 6.23: comparison of average yaw angle at diffuser exit between CFD and test close to surge, design and close to choke operating conditions.

flow is clearly visible in the yaw angle profiles when moving from choke to design point, the flow becomes more tangential at both hub and shroud. Instead the low momentum region close to hub side is visible for both design point and close to surge conditions with very close values. At the shroud side the angle is more tangential for the close to surge condition due to the strong adverse pressure gradient at the end of the diffuser.

Boundary layer development in those areas are especially difficult to simulate be-

cause they are usually formed by a combination of boundary layer growth, secondary flows and leakage flows. As a result the boundary layer skewness introduces streamwise vorticity, which has a large effect on the secondary flow in the downstream blade rows.

To also take into account the effect of diffuser modeling when vanes are present, another test case for a bi-dimensional impeller at ow flow coefficient stage with vaned diffuser is show in figure 5.18. Figure 6.24 shows the spanwise, tangentially averaged, flow angle profile at diffuser inlet for high fidelity CFD and standard one at design point, close to choke (right limit) and close to stall (left limit) operating points.

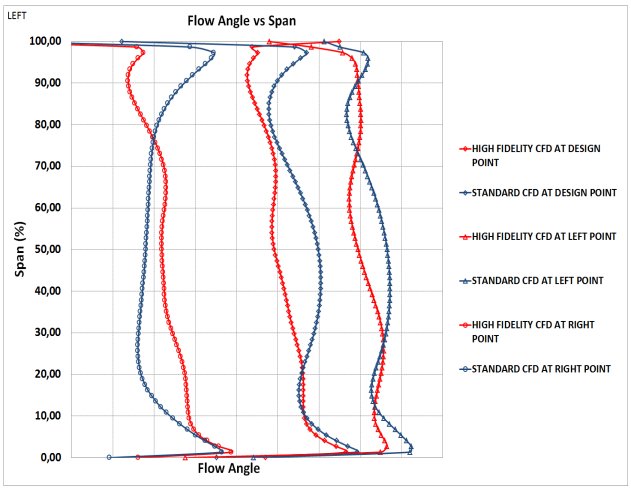

Figure 6.24: Flow angle profile at diffuser inlet for high fidelity and standard CFD at different operating points.

It is evident from the comparison that low momentum, high tangential flow is sucked inside the shroud cavity for all the operating points. The same effect happens for the back-side cavity even if to a lesser extent than the front-side one. Figure 6.25 shows the contours of $V_M \cdot |V_r|$ inside the diffuser for the high fidelity and standard one cases close to stall operating point. The horizontal black line represents the position of the vanes leading edge into the diffuser.

Even if it is well known that the mixing plane approach under-estimates separated shroud region at diffuser inlet that is a relevant feature in surge margin assessment, it is clear from the figure that the an area of low radial velocity flow is present at diffuser inlet close to the endwalls in case of leakge flows due to the strong diffuser/cavities interaction. Instead for the no leakages simulations the area is not present and the flow develops inside

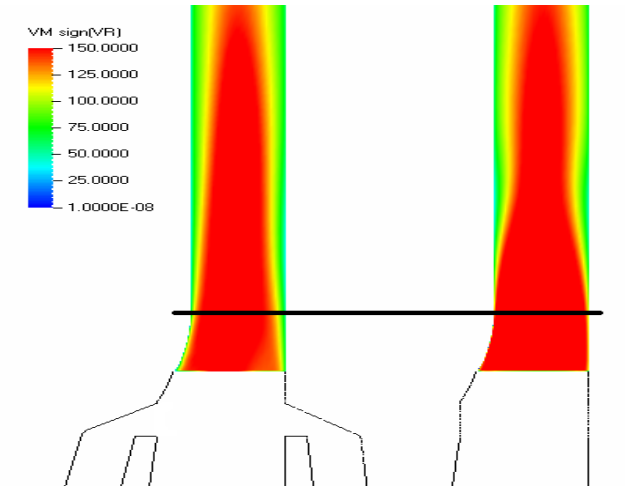

Figure 6.25: Contours of radial velocity inside the diffuser after the mixing plane position for the high fidelity and standard CFD respectively.

the diffuser without any interaction.

Also, when diffuser is choked, the correct computation of the total pressure profile at impeller exit is fundamental for the right limit assessment since diffuser throat area, aerodynamic blockage and gas properties do not vary significantly. Cavity flows modeling was found to be important for these purposes.

Finally in figure 6.26 is shown the trend of static pressure recovery coefficient inside the diffuser for the CFD with and without leakage flows included across the stage operating range. The static pressure recovery coefficient is calculated as shown in equation (6.2). The black vertical line indicates the stage design flow coefficient, the horizontal one the 0 in the Cp scale.

$$Cp = \frac{Ps_{40} - Ps_{20}}{Pt_{20} - Ps_{20}} \tag{6.2}$$

It worth nothing here that in case of no cavities modeled inside the domain the diffuser shows a recovery also close to deep choke whereas the CFD with leakge flows included shows an acceleration inside the diffuser. Also towards the left limit the CFD with cavities flow included tends to be more conservative and closer to test data.

Moving from impeller exit to diffuser outlet, previous analysis on vaneless diffusers show that there is a strong interaction bewteen leakage flows and diffuser and that only

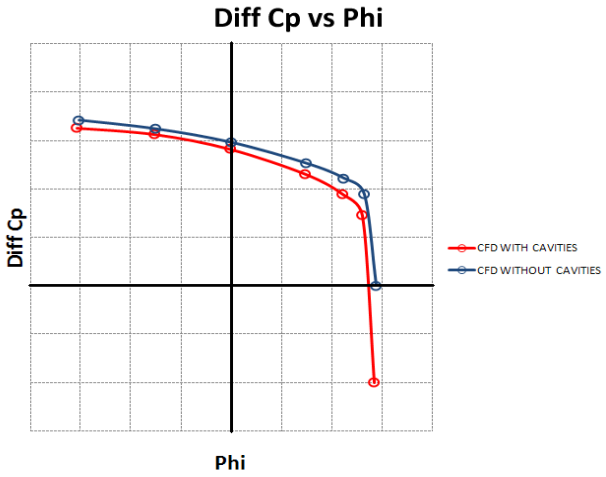

Figure 6.26: Static pressure recovery coefficient inside the diffuser for the CFD with and without leakage flows included across the stage operating range.

modeling cavities inside the domain is possible to understand correctly flow behavior and accurately predict the performance. In particular the low momentum, high tangential flow is sucked inside the cavities and an area of recirculating/mixing flow develops after the impeller trailing edge. This translates in a lower static pressure diffuser recovery due to the increase of separated regions close to the endwalls with fallouts in the downstream components performance. Diffuser inet metal angle distribution designed for a non perturbated flow would lead to a wrong assessment of stationary components behavior.

Finally, when vanes are installed into the diffuser, and velocity profiles at diffuser exit are less affected by the modeling of cavities because are more influenced by the turning given by the blades. Furthermore, the necessity to interpose a mixing plane between impeller trailing edge and diffuser leading edge due to different periodicity of the blades smooth out the circumferential effects of the cavity flows presence on downstream stationary components. Finally, it is well know that outlet scroll imposes a strong circumferential non-uniformities throughout the compressor and provides a downstream volume that can allow surge and so it is necessary to model it for compressor dynamic behavior assessment at surge. Nevertheless it was found in this case that static pressure distortions at section 40 were below 3% with respect to average value, i.e. the distribution of static pressure was quite uniform at diffuser exit.

6.3 Return Channel Flow

The correct modeling of flow phenomena at diffuser exit is very important for the optimization of return channel. In particular Smirnov et al. [7] showed improvements in flow modeling using the SST turbulence model with a curvature correction method and in particular in the U-bend region. Kowalski et al. [40] using standard CFD showed a big separated region in the U-bend of a centrifugal compressor stage that has never been found in experimental activities as per author's knowledge.

Figure 6.27 shows the non dimensional circumferentially averaged contours of meridional velocity from diffuser inlet (after leakage cavities interfaces) up to U-bend exit for the standard CFD high fidelity CFD respectively at design mass flow rate. Test case reported here is the one described in figure 5.2

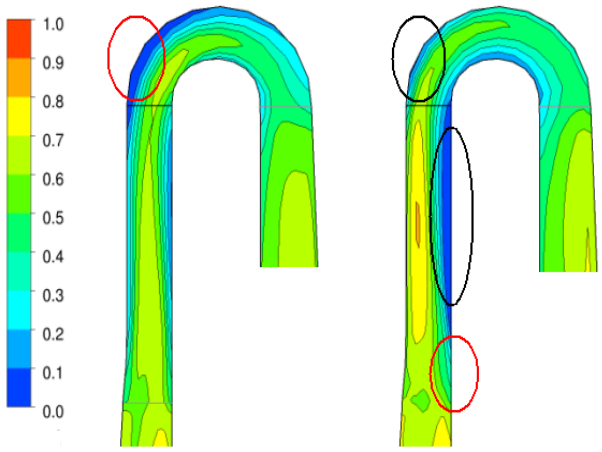

Figure 6.27: Circumferential averaged meridional velocity contours from standard CFD (left) and high fidelity CFD (right) at design point.

The flow field for the standard CFD shows a big area of low momentum flow close to the shroud side in the U-bend region reported in the red circle in the picture. Instead the case with cavities modeling does not show this phenomenon. The effect of the re-entering flow at hub side is clearly visible (in red circle). The effects on the flow profiles at impeller trailing edge were discussed in the previous paragraphs; furthermore the high swirling flow pushes the main flow towards the shroud side. This affects the flow behavior downstream where a region of low momentum flow develops close to the diffuser hub (reported in black

circle at hub side) due to the mixing of cavity flow with main-stream. Further downstream the low momentum region at shroud side inside the U-bend region reduces significantly (in black circle at shroud side of the U-bend).

Figure 6.28 and 6.29 shows the non dimensional circumferential averaged contours of meridional velocity from diffuser inlet (after leakage cavities interfaces) up to U-bend exit for the standard CFD and high fidelity CFD respectively close to stall and close to choke.

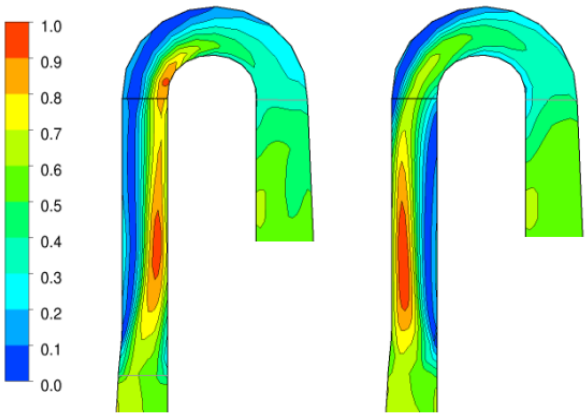

Figure 6.28: Circumferentially averaged meridional velocity contours from standard CFD (left) and high fidelity CFD (right) close to stall point.

The first thing that can be observed, as expected, is the major influence of leakage flows modeling close to stall with respect to close to choke operating condition. In fact close to choke the amount of leakage flow through the cavities is much smaller with respect to close to stall as showed before for both hub and shroud cavities. This results in a lower influence on flow features differences between the case with and without cavities. However similar conclusions to the design point condition can be drawn even if at a lower extent.

Close to stall condition, the difference in the circumferentially averaged meridional velocity contour plot is remarkable between standard CFD and high fidelity one. In the standard CFD, the flow is attached to the diffuser hub and a large low velocity zone is visible close to the diffuser shroud. The flow starts to separate in the diffuser pinch area and develops all across the diffuser and U-bend zones. On contrary, in the high fidelity CFD, low velocity zone can be seen close to the diffuser hub wall and main flow is pushed towards the shroud side. Anyhow the flow starts to detach from shroud wall close to the

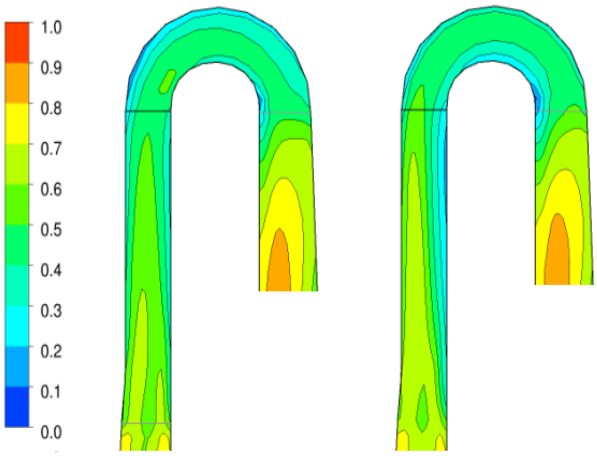

Figure 6.29: Circumferentially averaged meridional velocity contours from standard CFD (left) and high fidelity CFD (right) close to choke point.

diffuser end due to the strong adverse pressure gradient; the separation seems to be a real aerodynamic situation and different from what found at design point condition for the case without cavities.

Figure 6.30 shows the component by component losses for the standard CFD and high fidelity CFD. The effects of leakage flows are clearly shown all across the compressor stage in reducing the efficiency with respect to the case without. As expected, the main difference is found in the impeller, where the compressed gas leaks through the shroud cavity re-entering in the main flow at impeller inlet. The difference in flow profiles at diffuser inlet as shown before affects the diffuser losses, which in the case of cavities modeling are due to mixing zone and low momentum areas. Losses in the return channel are also affected by the flow leaving the main-stream at hub trailing edge even if at a lesser extent. U-bend is the only component that shows higher efficiency in case of CFD with cavities modeling, the reduced low momentum zone close to the shroud side can be responsible of this effect as also confirmed by flow profiles at diffuser exit showed in Figures 6.16, 6.17 and 6.18.

Finally the comparison between test and high fidelity CFD for the total pressure loss coefficient in the return channel is shown in Figure 6.31. The total pressure loss coefficient is calculated as shown in equation (6.3).

$$\xi = \frac{Pt_{60} - Pt_{40}}{Pt_{40} - Ps_{40}} \tag{6.3}$$

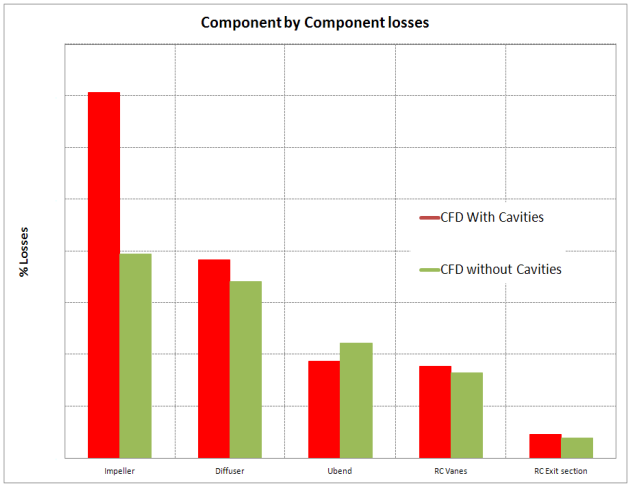

Figure 6.30: Component losses from CFD with and without cavities modeling at design point.

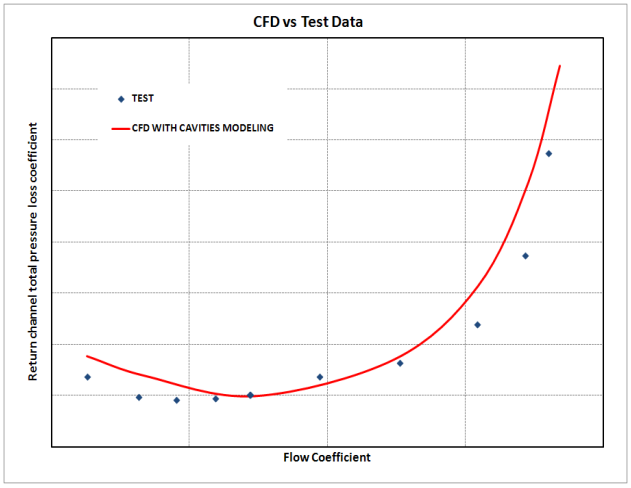

Figure 6.31: Total pressure loss coefficient in return channel for test and high fidelity CFD.

It is well know that 1D model of return channel are not able to capture accurately the losses across the entire compressor operating range. This is due to the weak correlations of flow properties, e.g. flow angle, between impeller and return channel. Furthermore it has been shown that standard CFD is not able to capture accurately the flow profiles at the diffuser exit, leading into a wrong assessment of return channel losses. Instead, highfidelity CFD enabled capturing the flow behavior and overall losses all across the stage operating conditions with a good accuracy, especially at overflow.

6.4 Cavity Flow

The modeling of the entire cavities allows to have a deeper insight in the leakages flow field. Direction of flow stream, in a single stag compressor, is always from trailing edge to leading edge in the shroud cavity; instead for the hub one the direction depends on the balance between pressure drop from impeller trailing edge to return channel trailing edge and static pressure recovery of stationary components. Static pressure recovery coefficient is calculated as per equation (6.4):

$$cp = \frac{Ps_{60} - Ps_{20}}{Pt_{20} - Ps_{20}} \tag{6.4}$$

At compressor operating conditions where the pressure recovery coefficient is positive the flow direction is from return channel to impeller, vice versa if negative. At design operating point and towards left limit the pressure recovery coefficient is positive. Towards right operating limit at a certain flow coefficient the increase of total pressure losses due to skin friction becomes too high with respect to the stationary components static pressure recovery and the flow inverts the direction.

Moreover, the flow in balance drum or inter-stage leakages is always from the higher pressure section to the lower one. The flow there is similar to what will be described for single stage.

In both shroud and hub cavities, inner wall rotates at the same peripheral speed of the impeller, instead the outer one is stationary.

Figure 6.32 shows contours of entropy with streamlines super-imposed for the front cavity of a bi-dimensional low flow coefficient stage at high peripheral Mach number in over-hung configuration, described in figure 5.18. It is clear that there is a strong area of recirculating flow in proximity of the shroud interface. Reverse flow that forms across the interface is well captured by the numerical model. In fact the effect of the rotating blades is counteracted by the recirculating flow in the cavity. The impeller pushes the flow inside the cavity but the presence of labyrinth seals mitigate the amount of flow passing through that recirculates close to the impeller trailing edge. Figure 6.33 shows contours of entropy with streamlines super-imposed for the front cavity labyrinth seals. Jets form between teeth and lower faces, instead cavity vortices establish between different teeth. Steps in the cavity geometry are used to destroy jets continuity.

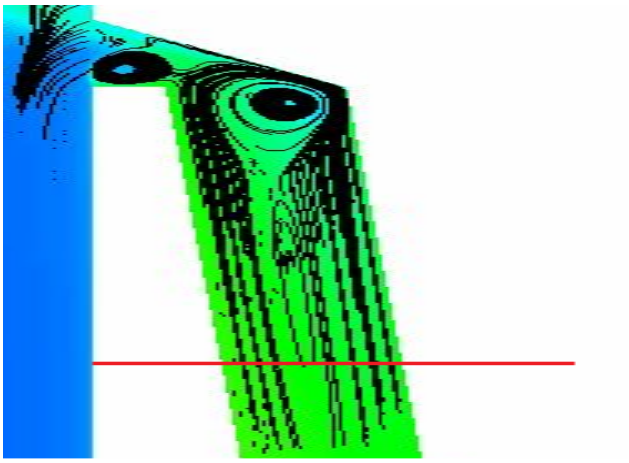

Figure 6.32: Contours of entropy with streamlines super-imposed for the front cavity.

Figure 6.33: Contours of entropy with streamlines super-imposed for the front cavity labyrinth seals.

Figure 6.34, 6.35 and 6.36 show respectively axial, radial and tangential velocity inside the forward cavity in the area at mid distance between cavity flow inlet and labyrinth seals marked with a read line in figure 6.32. In figures 6.34, 6.35 and 6.36 the non dimensional span is referred to the no dimensional distance between stationary and rotating walls inside the cavity. Fluid particles close to the inner wall due to the no-slip condition have a tangential velocity that is the same of the rotating wall and so centrifugal force much

higher than the ones close to the outer wall that are at rest. As expected axial velocity is the one with lowest magnitude. Radial velocity increases rapidly from 0 at the wall to the maximum close to the wall and then becomes zero again at the center region; opposite walls have opposite radial velocity direction. The flow is anti-symmetric with a very small negative total average radial velocity due to the net leakage flow leaving the cavity. Static pressure inside the cavity is almost equal along the axial and circumferential direction and decreases gradually in the radial one moving downwards. An highly complex fluid structure develops and three main regions can be distinguished based on previous statements: a core flow and two opposite areas close to the walls. The core flow has essentially zero velocity gradient as shown in the radial velocity profiles. The core flow can have different vortex structures depending mainly on the cavity geometry. The fluid close to the rotating wall is centrifuged towards the cavity inlet whereas the fluid close to the outer wall is moved downwards. A perfectly corresponding behavior can be described for the rear cavity.

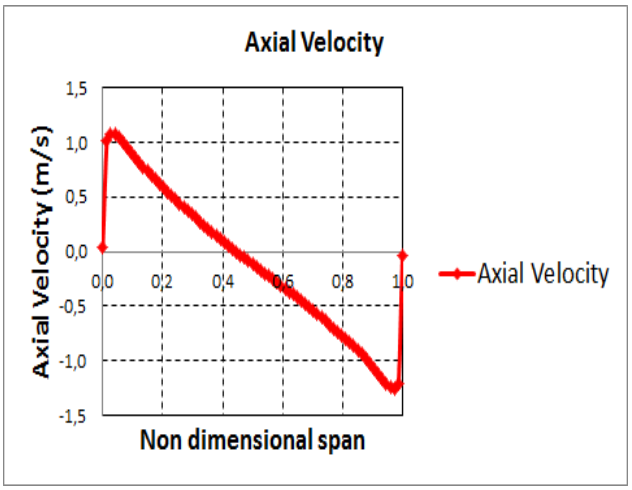

Figure 6.34: Axial velocity distribution inside the forward cavity.

Figures 6.37 and 6.38 show the comparison between test data and CFD for static pressure variation inside the cavities at the inner and outer walls versus non dimensional radius for a medium flow coefficient stage in intermediate stage configuration. Radius 0 is the minimum cavity radius and 1 is the maximum. The experimental data are area averaged between two redundant probes for each measurement point. Figure 6.39 shows the position of the static pressure probes inside both the cavities at hub and shroud for a typical case.

From CFD is clearly visible the pressure drop across the teeth seals for both cavities

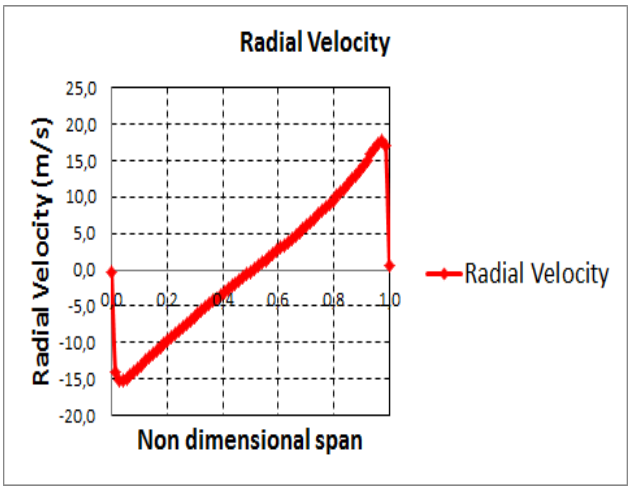

Figure 6.35: Radial velocity distribution inside the forward cavity.

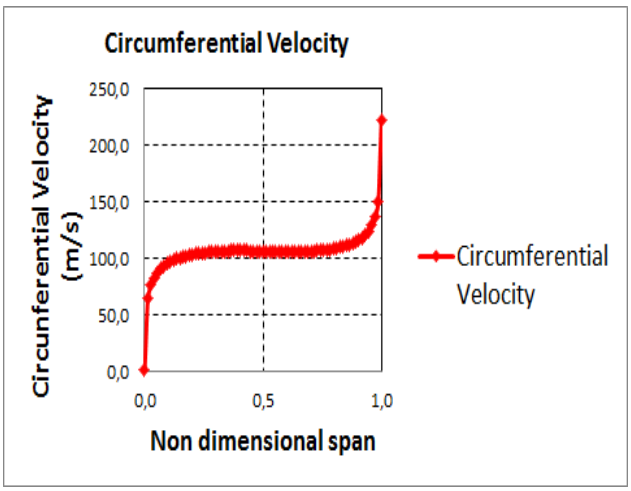

Figure 6.36: Circunferential velocity distribution inside the forward cavity.

that is well captured. Generally the agreement between test and simulation is good. From the static pressure drop across the cavity in the test data is possible to estimate the leakage mass flows. At design point leakage mass flows are 0.6% and 0.15% of the total mass flow respectively for shroud and hub cavities. This was found to be in very good agreement with CFD as can be inferred from the static pressure distribution. For simulations with coupled hub cavity and source terms like the one in the study of Sun [13], the static pressure distribution is highly dependent on the prescribed mass flow that is not known a priori;

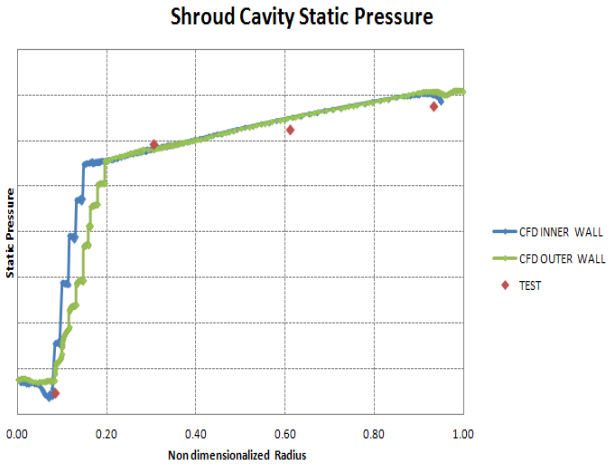

Figure 6.37: Static pressure variation across the shroud cavity for CFD and experimental data.

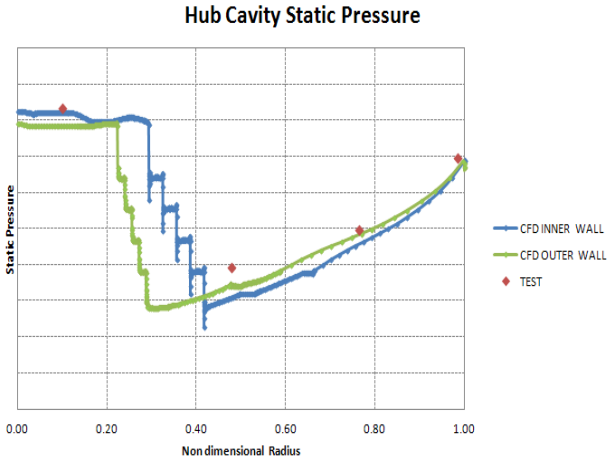

Figure 6.38: Static pressure variation across the hub cavity for CFD and experimental data.

usually a trial and error method is used until the expected pressure drop across the cavity is found. Instead in this case, modeling all the cavity domain, no source terms needs to be prescribed and the accuracy of the simulation greatly improves. Static pressure at hub cavity on the return channel side is higher than the one close to impeller trailing edge and this is connected to flow direction as explained before. It is also clear from the static pressure distribution in the hub cavity the pumping effect of fluid after the seal labyrinths.

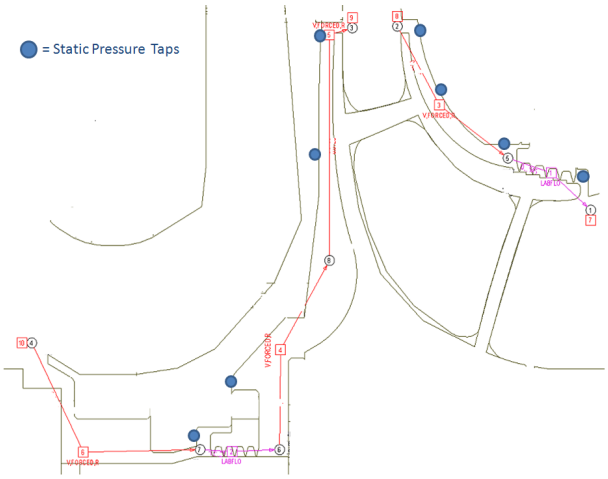

Figure 6.39: Position of the static pressure probes inside both the cavities at hub and shroud for a typical case.

Furthermore the agreement between test and computational data allows to expect that the amount of recirculating mass flow inside the shroud cavity is correctly assessed by CFD. Axial thrust is another important information for bearings selection and rotordynamic verification. The agreement in static pressure distribution between test and CFD allows to derive important correlations for a priori verification. Prediction tools for leakage effects can be tuned based on CFD results.

Chapter 7

Conclusions

Aim of this thesis was to push CFD capabilities toward virtual testing. In other words, this thesis describes a methodology by which virtual tests can be conducted on single stages and multistage centrifugal compressors in a similar fashion to a typical test rig. In fact, in the vision of the author, CFD represents nowadays an exceptional tool for centrifugal compressors performance prediction and flow phenomena understanding.

7.1 Summary

Several centrifugal compressor single stages, ranging across different inlet flow coefficients and peripheral Mach numbers, applied to disparate processes (e.g. LNG, pipeliners, barrel compressors, etc), as well as applications of multistage compressors, were selected as test cases for this study. Both steady and unsteady simulations were conducted in order to fully capture the time averaged and time accurate operating conditions. Moreover, detailed geometrical features were faithfully reproduced in the computational domain and advanced numerical models were used in the setup with accuracy not possible before.

CFD predictions were compared with test results regarding both overall performance and detailed flow features. Advantages of this approach is the reduced cost with respect to tests and the possibility to virtually instrument the machine all along the computational domain where it is not possible in the real compressor.

Results of the present study can be summarized as follow:

- The so called high fidelity CFD is able not only to predict with an outstanding accuracy overall compressor performance but also to reproduce local detailed flow features.

- Particular care needs to be put in modeling accurately all the single components of the centrifugal compressor. In prticular, geometrical features like fillets, leakages flows, leading edge and trailing edge discretization need to be faithfully reproduced into the computational domain.

- Numerical algorithms need to be at the state of the art. Turbulence models, curvature correction, roughness treatment, boundary conditions and real gas model are the main actors for the final outcome.

7.2 Recommendations and Future Work

Even if nowadays CFD is mature enough to represent a realible tool for centrifugal compressors modeling, many areas need to be further explored and developed. Some working in progress are reported here below:

- Unsteady simulations of full multistage centrifugal compressors are still too expensive for common industrial applications. However, with the exponential increase in infrastructures happened in the recent years, in the vision of the author, this will become reality in few years.

- Boundary layer transition is almost impossible to predict accurately with RANS models. LES applications would solve many uncertainties but many years need to be passed before industrial applications will become available.

Bibliography

[1] Ferrara, G., Ferrari, L., and Baldassarre, L., 2006. "Experimental characterization of vaneless diffuser rotating stall. part v: influence of diffuser geometry on stall inception and performance". In ASME Turbo Expo 2006. ASME Paper GT-2006-90693.

[2] Persico, G., Gaetani, P., and Guardone, A., 2005. "Design and analysis of new concept fast-response pressure probes". In Measurements Science and Technology, 16(9), pp 1741-1750.

[3] Persico, G., Gaetani, P., and Guardone, A., 2005. "Dynamics calibration of fast-response probes in low-pressure shock tubes". In Measurements Science and Technology, 16(9), pp 1751-1759.

[4] Toni, L., Ballarini, V., Cioncolini, S., Persico, G., and Gaetani, P., 2010. "Unsteady flow field measurements in an industrial centrifugal compressor". In 39th Turbomachinery Symposium, pp 49-58.

[5] Hah, C., and Krain, H., 1990. "Secondary flows and vortex motion in a high-efficiency backswept impeller at design and off-design conditions". *Journal of Turbomachinery*, pp. 7–13.

[6] Smirnov, P., Hansen, T., and Menter, F., 2007. "Numerical simulation of turbulent flows in centrifugal compressor stages with different radial gaps". In ASME Turbo Expo 2007. ASME Paper 2007-27376.

[7] Smirnov, P., and Menter, F., 2008. "Sensitization of the sst turbulence model to rotation and curvature by applying the spalart-shur correction term". In ASME Turbo Expo 2008. ASME Paper 2008-50480.

[8] Bourgeois, J. A., Martinuzzi, R. J., Savory, E., and Zhang, C., 2011. "Assessment of turbulence model predictions for an aero-engine centrifugal compressor". *Journal of Turbomachinery*, p. 133.

[9] Sorokes, J., Vezier, C., Pacheco, J., and Fakhri, S., 2012. "An analytical and experimental assessment of a diffuser flow phenomenon as a precursor to stall". In ASME Turbo Expo 2012. ASME Paper 2012-69122.

[10] Guidotti, E., Tapinassi, L., Toni, L., Bianchi, L., Gaetani, P., and Persico, G., 2011. "Experimental and numerical analysis of the flow field in the impeller of a centrifugal compressor stage at design point". In ASME Turbo Expo 2011. ASME Paper 2011-45036.

[11] Hunziker, R., Dickmann, H., and Emmerich, R., 2001. "Numerical and experimental investigation of a centrifugal compressor with an inducer casing bleed system". *Journal of Power and Energy,* **215(6)**, September, pp. 783–791.

[12] Tamaki, H., 2010. "Effect of recirculation device on performance of high pressure ratio centrifugal compressor". In ASME Turbo Expo 2010. ASME Paper 2010-22570.

[13] Sun, Z., Tan, C., and Zhang, D., 2009. "Flow field structures of the impeller backside cavity and its influences on the centrifugal compressor". In ASME Turbo Expo 2009. ASME Paper 2009-59879.

[14] Mischo, B., Seebass-Linggi, C., Ribi, B., and Mauri, S., 2009. "Influence of labyrinth seal leakage on centrifugal compressor performance". In ASME Turbo Expo 2009. ASME Paper 2009-59524.

[15] Wang, Z., Xu, L., and Xi, G., 2010. "Numerical investigation of the labyrinth seal design for a low flow coefficient centrifugal compressor". In ASME Turbo Expo 2010. ASME Paper 2010-23096.

[16] Guidotti, E., Tapinassi, L., Naldi, G., and Chockalingam, V., 2012. "Cavity flow modeling in an industrial centrifugal compressor stage at design and off-design conditions". In ASME Turbo Expo 2012. ASME Paper 2012-68288.

[17] Guidotti, E., Tapinassi, L., and Naldi, G., 2012. "Influence of seal leakages modeling on low flow coefficient centrifugal compressor stages performance". In ATI Congress 2012.

[18] Satish, K., Guidotti, E., Rubino, D., Tapinassi, L., and Prasad, S., 2013. "Accuracy of centrifugal compressor stages performance prediction by means of high fidelity cfd and validation using advanced aerodynamic probe". In ASME Turbo Expo 2013. ASME Paper 2013-95618.

[19] Lettieri, C., Baltadjiev, N., Casey, M., and Spakovszky, Z., 2013. "Low-flow-coefficient centrifugal compressor design for supercritical co2". In ASME Turbo Expo 2013. ASME Paper 2013-95012.

[20] Jameson, A., Schmidt, W., and Turkel, E., 1981. "Numerical solution of the euler equations by finite volume methods using runge-kutta time-stepping schemes". In AIAA 14th Fluid and Plasma Dynamics Conference.

[21] Holmes, D. G., Mitchell, B. E., and Lorence, C. B., 1997. "Three dimensional linearized navier-stokes calculations for flutter and forced response". In ISUATT Symposium.

[22] Kapetanovic, S. M., N., F. F., G., H. D., and M., O., 2007. "Impact of combustor exit circumferential flow gradients for gas turbine prediction". In In Proceedings of the 5th International Conference on Heat and Mass transfer.

[23] Wilcox, D. C., 1998. *Turbulence Modeling for CFD*. DCW Industries, Inc., La Cañada, CA.

[24] Launder, B. E., M., and Kato, 1993. "Modeling flow induced oscillations in turbulent flow around a square cylinder". In ASME FED, 57, pp 189-199.

[25] Grimaldi, A., Tapinassi, L., Biagi, F. R., Michelassi, V., Bernocchi, A., and Guenard, D., 2007. "Impact of inlet swirl on high-speed high-flow centrifugal stage performance". In ASME Turbo Expo 2007. ASME Paper GT-2007-27202.

[26] Scotti, A. D. G., Biagi, F. R., Sassanelli, G., and Michelassi, V., 2007. "A new slip factor correlation for centrifugal impellers in a wide range of flow coefficients and peripheral mach numbers". In ASME Turbo Expo 2007. ASME Paper GT-2007-27199.

[27] Aalburg, C., Simpson, A., Schmitz, M. B., Michelassi, V., Evangelisti, S., Belardini, E., and Ballarini, V., 2008. "Design and testing of multistage centrifugal compressors with small diffusion ratios". In ASME Turbo Expo 2008. ASME Paper GT-2008-51263.

[28] Ramakrishnan, K., Richards, S., Moyroud, F., and Michelassi, V., 2011. "Multi-blade row interactions in a low pressure ratio centrifugal compressor stage with vaned diffuser". In ASME Turbo Expo 2011. ASME Paper 2011-45932.

[29] Guidotti, E., Satish, K., Rubino, D., Tapinassi, L., Prasad, S., Toni, L., and Naldi, G., 2014. "Influence of cavity flows modeling on centrifugal compressor stages performance prediction across different flow coefficient impellers". In ASME Turbo Expo 2014. ASME Paper 2014-25830.

[30] Erdos, J. I., Alzner, E., and McNally, W., 1997. "Numerical solution of periodic transonic flow through a fan stage". *AIAA Journal,* **15**(11), pp. 1559–1568.

[31] Suresh, A., and Rangwalla, A., 2012. "Stability of the phase-lag boundary condition in turbomachinery simulations". In 48th AIAA/ASME/SAE/ASEE Joint Propulsion Conference Exhibit 2012. 2417-2425.

[32] Denton, J., 2010. "Some limitations of turbomachinery cfd". In ASME Turbo Expo 2010. ASME Paper 2010-22540.

[33] Cotroneo, J. A., Cole, T. A., and Hofer, D. C., 2007. "Aerodynamic design and prototype testing of a new line of high efficiency, high pressure, 50 In ASME Turbo Expo 2007. ASME Paper GT-2007-27315.

[34] Mangani, L., Casartelli, E., and Mauri, S., 2012. "Assessment of various turbulence models in a high pressure ratio centrifugal compressor with an object oriented cfd code". *Journal of Turbomachinery*, p. 134(6).

[35] Panizza, A., Sassanelli, G., iurisci, G., and Sankaran, S., 2012. "Performance uncertainty quantification for centrifugal compressors: 1. stage performance variation". In ASME Turbo Expo 2012. ASME Paper 2012-68036.

[36] Sankaran, S., Sassanelli, G., iurisci, G., and Panizza, A., 2012. "Performance uncertainty quantification for centrifugal compressors: 2. flange to flange variability". In ASME Turbo Expo 2012. ASME Paper 2012-68220.

[37] Panizza, A., Rubino, D., and Tapinassi, L., 2014. "Efficient uncertainty quantification of centrifugal compressor performance using polynomial chaos". In ASME Turbo Expo 2014. ASME Paper 2014-25081.

[38] Casey, M. V., Dalbert, P., and Roth, G., 1990. "The use of 3d viscous flow calculations in the design and analysis of industrial centrifugal compressors". ASME Paper 90 Gt-2.

[39] Clayton, R. P., Leong, W. U. A., Sanatian, R., Issa, R. I., and Xi, G., 1998. "A numerical study of the three-dimensional turbulent flow in a high-speed centrifugal compressor". ASME Paper 98 Gt-49.

[40] Kowalski, S., Pacheco, J. E., Fakhri, S., and Sorokes, J., 2012. "Centrifugal stage performance prediction and validation for high mach number applications". In 41th Turbomachinery Symposium.

Appendix A

List of Publications

In appendix A it is reported the list of publications that have been presented or submitted during this reserch work and object of the present thesis.

- Guidotti, E., Tapinassi, L., Toni, L., Bianchi, L., Gaetani, P., and Persico, G., 2011. "Experimental and numerical analysis of the flow field in the impeller of a centrifugal compressor stage at design point." In ASME Turbo Expo 2011. ASME Paper 2011-45036.

- Guidotti, E., Tapinassi, L., Naldi, G., and Chockalingam, V., 2012. "Cavity flow modeling in an industrial centrifugal compressor stage at design and off-design conditions." In ASME Turbo Expo 2012. ASME Paper 2012-68288.

- Guidotti, E., Tapinassi, L., and Naldi, G., 2012. "Influence of seal leakages modeling on low flow coefficient centrifugal compressor stages performance." In ATI Congress 2012.

- Satish, K., Guidotti, E., Rubino, D., Tapinassi, L., and Prasad, S., 2013. "Accuracy of centrifugal compressor stages performance prediction by means of high delity CFD and validation using advanced aerodynamic probe." In ASME Turbo Expo 2013. ASME Paper 2013-95618.

- Guidotti, E., Satish, K., Rubino, D., Tapinassi, L., Prasad, S., Toni, L., and Naldi, G., 2014. "Influence of cavity flows modeling on centrifugal compressor stages performance prediction across differentflow coefficient impellers." In ASME Turbo Expo 2014. ASME Paper 2014-25830.

- Guidotti, E., Baldassarre, L., Rubino, D., Tapinassi, L., 2014. "On the accuracy of centrifugal compressor systems performance prediction by means of high fidelity CFD." In 43rd Turbomachinery Symposium.